REPUBLIC OF TURKEY
ADANA ALPARSLAN TÜRKEŞ SCIENCE AND TECHNOLOGY UNIVERSITY

GRADUATE SCHOOL OF NATURAL AND APPLIED SCIENCES
DEPARTMENT OF ELECTRICAL AND ELECTRONIC ENGINEERING

MODELING AND ANALYSIS OF FIVE-PORT ISOLATED BIDIRECTIONAL DC-DC CONVERTER FOR INTERFACING PV/FC/BATTERY SYSTEMS WITH BIPOLAR DC MICROGRIDS

ELANUR EKİCİ
MASTER OF SCIENCE

ADANA 2022

REPUBLIC OF TURKEY
ADANA ALPARSLAN TÜRKEŞ SCIENCE AND TECHNOLOGY UNIVERSITY

GRADUATE SCHOOL OF NATURAL AND APPLIED SCIENCES
DEPARTMENT OF ELECTRICAL AND ELECTRONIC ENGINEERING

MODELING AND ANALYSIS OF FIVE-PORT ISOLATED BIDIRECTIONAL DC-DC CONVERTER FOR INTERFACING PV/FC/BATTERY SYSTEMS WITH BIPOLAR DC MICROGRIDS

ELANUR EKİCİ
MASTER OF SCIENCE

SUPERVISOR
ASST. PROF. DR. TAHSİN KÖROĞLU
COSUPERVISOR
ASST. PROF. DR. MURAT MUSTAFA SAVRUN
ADANA 2022

I hereby declare that all information in this thesis has been obtained and presented in accordance with academic rules and ethical conduct. I also declare that, as required by these rules and conduct, I have fully cited and referenced all information that is not original to this work.

[Signature]

Elanur EKİCİ

ABSTRACT

MODELING AND ANALYSIS OF FIVE-PORT ISOLATED BIDIRECTIONAL DC-DC CONVERTER FOR INTERFACING PV/FC/BATTERY SYSTEMS WITH BIPOLAR DC MICROGRIDS

Elanur EKİCİ

Department of Electrical and Electronic Engineering

Supervisor: Asst. Prof. Dr. Tahsin KÖROĞLU

Co-Supervisor: Asst. Prof. Dr. Murat Mustafa SAVRUN

January 2022, 78 pages

In this thesis, a novel five-port, three-input and dual-output, isolated bidirectional DC-DC converter (FPIBC) topology with an effective control system for power sharing and voltage balancing in bipolar DC microgrids (BPDCMGs) is presented. The proposed converter acts as the interface for the integration of a hybrid generation system comprised of the fuel cell (FC), the photovoltaic (PV) system, and the battery to BPDCMGs. The FPIBC consists of two full-bridge converters, a resonant tank, a high-frequency transformer (HFT), and a voltage balancer circuit. The symmetrical bipolar output voltages are ensured by a voltage balancer circuit composed of a fully controlled switch and four diodes, without any need for an additional converter. Less number of circuit elements are used in the proposed converter compared to the existing converters. A simulation model has been developed using the MATLAB/Simulink program to verify the effectiveness and usefulness of the aforementioned converter. Different case studies have been carried out under conditions of altered FC pressure, solar irradiation, battery charge/discharge status, load change and voltage imbalance to test the performance of the proposed converter. The performance of the system and the efficiency are verified with simulation results. The simulation results revealed that the system has an efficiency of at least 91.13% during case studies, the voltage imbalance was kept below 1%, and bidirectional power transmission function is performed successfully.

Keywords: multiport converter, dc-dc converter, bipolar dc microgrid, voltage balancer, renewable energy integration

ÖZET

BİPOLAR DA MİKROŞEBEKELER İLE FOTOVOLTAİK/YAKIT HÜCRESİ/BATARYA SİSTEMLERİNİN ARAYÜZLENMESİ İÇİN BEŞ PORTLU İZOLELİ ÇİFT YÖNLÜ DA-DA DÖNÜŞTÜRÜCÜNÜN MODELLENMESİ VE ANALİZİ

Elanur EKİCİ

Elektrik Elektronik Mühendisliği Anabilim Dalı

Danışman: Dr. Öğr. Üyesi Tahsin KÖROĞLU

İkinci Danışman: Dr. Öğr. Üyesi Murat Mustafa SAVRUN

Ocak 2022, 78 sayfa

Bu tezde, bipolar DA mikroşebekelerde güç paylaşımı ve gerilim dengelemesi için etkin bir kontrol sistemine sahip yeni bir beş portlu, üç girişli ve çift çıkışlı, izoleli çift yönlü DA-DA dönüştürücü topolojisi sunulmuştur. Önerilen dönüştürücü fotovoltaik sistem, yakıt hücresi ve bataryadan oluşan bir hibrit üretim sisteminin bipolar DA mikro şebekelere entegrasyonu için arayüz görevi üstlenmektedir. Beş portlu izoleli çift yönlü DA-DA dönüştürücü (FPIBC) iki tam köprü dönüştürücü, bir rezonans tankı, bir yüksek frekanslı transformatör (HFT) ve bir gerilim dengeleyici devresinden oluşur. Simetrik bipolar çıkış gerilimleri ek bir dönüştürücüye ihtiyaç duyulmadan bir anahtar ve dört diyottan oluşan gerilim dengeleyici devresi ile sağlanmıştır. Önerilen dönüştürücüde literatürdeki mevcut dönüştürücülere göre daha az sayıda devre elemanı kullanılmıştır. Bahsedilen dönüştürücünün etkinliğini ve kullanılabilirliğini doğrulamak için MATLAB/Simulink programı kullanılarak bir simülasyon modeli geliştirilmiştir. Önerilen dönüştürücünün performansını test etmek için değişen yakıt hücresi basıncı, güneş ışınımı, batarya şarj/deşarj durumu, yük değişimi ve gerilim dengesizliği koşulları altında farklı vaka çalışmaları gerçekleştirilmiştir. Sistemin performansı ve sağladığı verimlilik değerleri simülasyon sonuçları ile doğrulanmıştır. Simülasyon sonuçları, vaka çalışmalarına göre sistemin en az %91,13 verimliliğe sahip olduğunu, gerilim dengesizliğinin %1'in altında tutulduğunu ve çift yönlü güç aktarımı işlevinin başarıyla yerine getirildiğini ortaya koymuştur.

Anahtar Kelimeler: çok portlu dönüştürücü, da-da dönüştürücü, bipolar da mikroşebeke, gerilim dengeleyici, yenilenebilir enerji entegrasyonu

Dedication

I would like to dedicate my thesis to my family.

ACKNOWLEDGEMENTS

I would like to express my heartfelt thanks to Asst. Prof. Dr. Tahsin KÖROĞLU for his supervision, guidance, great support, extremely valuable advice and encouragements throughout this thesis. It has been a great honor to have Asst. Prof. Dr. Tahsin KÖROĞLU as supervisor.

I am also grateful to my co-supervisor Asst. Prof. Dr. Murat Mustafa SAVRUN for his guidance, strong support, extremely useful suggestions and criticism throughout in the thesis. His technical assistance and personal advice have been invaluable.

I would also like to thank Assoc. Prof. Dr. Mehmet Uğraş CUMA, Assoc. Prof. Dr. Mustafa İNCİ and Asst. Prof. Dr. Zehan KESİLMİŞ for accepting to be the member of examining committee for my thesis.

I am also grateful to the members of the Electrical and Electronic Engineering Department, Adana Alparslan Türkeş Science and Technology University.

Finally, I wish to express my deepest gratitude to my parents and my brother for their endless support, encouragement and patience.

TABLE OF CONTENTS

LIST OF FIGURES

LIST OF TABLES

NOMENCLATURE

AC	: Alternating Current
BPDCMG	: Bipolar DC Microgrid
DC	: Direct Current
DG	: Distributed Generation
ESU	: Energy Storage Unit
FC	: Fuel Cell
FHA	: Fundamental Harmonic Approximation
FPIBC	: Five Port Isolated Bidirectional DC-DC Converter
HFT	: High-Frequency Transformer
IGBT	: Insulated Gate Bipolar Transistor
MOSFET	: Metal Oxide Semiconductor Field Effect Transistor
MPC	: Multiport Converter
MPP	: Maximum Power Point
MPPT	: Maximum Power Point Tracking
PI	: Proportional-Integral
PV	: Photovoltaic
PVM	: Pulse Width Modulation
RES	: Renewable Energy Source
SEPIC	: Single-Ended Primary-Inductor Converter
SOC	: State of Charge
SOFC	: Solid Oxide Fuel Cell
SPS	: Single Phase Shift
ZCS	: Zero Current Switching
ZVS	: Zero Voltage Switching

1. INTRODUCTION

1.1. Distributed Generation

In the last decades, traditional power systems have been faced with problems such as depletion of fossil resources, high cost of energy, low energy efficiency and increasing environmental concerns. These problems have initiated research on interfacing renewable energy sources (RESs) such as wind power, photovoltaic cells, fuel cells and connecting them being integrated into the power grid in the form of distributed generation (DG) (Li and Kao, 2009). The power systems comprise centralized and distributed generation sources, building the generation stage. Renewable energy technologies, energy storage systems, power converters and loads are the main components of distributed power generation systems.

A microgrid is formed with an organized structure of the DG systems. The main goal of microgrids is to offer a new concept as an alternative to traditional centralized power grids by combining the benefits of low-carbon RESs with high-efficiency hybrid power systems. Recent studies point out that DC microgrids, in which RESs can be integrated more easily than AC microgrids, enhance reliability and efficiency (Dragičević et al., 2016). To improve the reliability and power quality, bipolar type DC microgrids that offer two voltage levels in a three-wire DC line (positive, negative, and neutral) have been introduced (Kakigano, Miura, and Ise, 2010).

The DG systems based on RESs and energy storage units (ESUs) are interfaced to the DC microgrid via power electronics converters. To integrate multiple RESs and ESUs simultaneously into DC microgrids, a large number of independent power electronics converters would be necessary. Nevertheless, such a configuration brings about low efficiency, high cost, and difficulties in centralized control (Tian et al., 2020). Multiport converters (MPCs) have recently come into prominence as they put forward an effective solution in the integration of multiple RESs and ESUs by the advantages of using a lower number of switches, fewer costs, higher efficiency, higher power density and less complexity in control.

In this chapter, power generation systems/distributed generation, and microgrids are introduced; general information about RESs and ESUs are given; structures of photovoltaic

(PV) panel, fuel cell (FC) and battery are reported. Then, the classification and operating principles of fundamental DC-DC converter topologies are presented.

1.2. Microgrids

With the development of modern power systems, new concepts such as the DG systems based on RESs, smart grids, microgrids and their control/management have attracted attention from the researchers and investigations on these topics have become greatly increased in the last decade. DG refers to electricity generation and energy storage at low or medium voltage levels (1-34,5kV). DG includes local power plants close to consumer centers, ESUs, and RESs such as wind energy, solar power, and FC (Wang et al., 2017). Microgrids are an organized form of these DG components.

Microgrids can also be defined as a variety of localized electrical systems that is independent from the main grid. Microgrids play a critical role in terms of providing high reliability, flexibility, high efficiency and reduced transmission line losses for interfacing multiple RESs and ESUs simultaneously.

DC microgrid, AC microgrid and AC-DC hybrid microgrid are three types of microgrid. DC microgrids and AC-DC hybrid microgrids are emerging concepts compared to AC microgrids. It is preferable to use DC microgrids in generation systems since they do not include frequency and phase components (Kabalci, Irgan, and Kabalci, 2018). Beyond the advantages such as absence of problems such as synchronization and reactive power, DC microgrids are of interest due to the features of high efficiency and reliability (Dragičević et al., 2016) (Ferrera et al., 2015). There are several studies carried out on these types of microgrids in the literature. It has been understood that DC microgrids have two configurations such as unipolar DC bus configuration and bipolar DC bus configuration (Wang et al., 2017).

1.3. Renewable Energy Sources and Energy Storage Units

Due to increasing environmental pollution and depletion of fossil fuels, utilization of renewable energy sources is increasing in microgrids, electric vehicles, aircraft, and other power electronics applications. Solar, wind, hydrogen, hydroelectric, wave, biomass and geothermal are the examples of renewable energies that are widely used. With the increasing usage of renewable energy, the greenhouse effect decreases due to low carbon emissions and the

minimum environmental pollution is provided. The advantages of renewable energy are as follows:

- The dependence of countries on petroleum derived energies decreases due to local electricity production.
- It becomes possible to feed the places where grid electricity cannot reach.
- Provides support to the country's economies by creating new employment areas.
- Allows more clean air with emission-free energy.
- Helps to achieve sustainable environment as they have unlimited reserves in nature.
- Provides more cheaper solutions compared to fossil fuels.

1.3.1. Solar Energy Systems

Solar energy is one of the most important and researched types of renewable energy. The solar energy that is delivered to the world through small energy units called photons is converted into electrical energy using semiconductor technologies in photovoltaic cells. With the scientific and technological developments, the use of solar energy is increasing globally. Solar energy can be utilized for a wide variety of applications including electric vehicles, hybrid energy systems, transportation, agricultural irrigation pumping systems and rural electrification.

The operating principle of PV panels is similar to a diode which simply consists of a p-n junction. Equivalent circuit of a solar panel is illustrated in Figure 1.1. Based on the photoelectric phenomenon principle, electrons detached from a metal move in the joint and form an electric current. The most commonly used materials in the structure of the PV panel are semiconductor materials such as silicon and gallium arsenide.

The power obtained from solar panels depends on the number of cells and connection types of the cells. Solar cells can be connected in two ways such that serial or parallel. Solar panels

includes solar modules which are formed from a large number of solar cells. The solar array is formed by the connection of these solar panels.

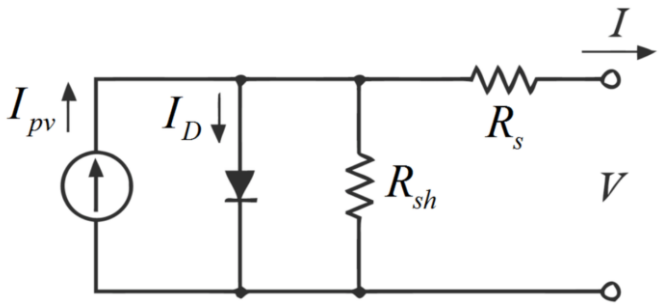

Figure 1.1. Equivalent circuit of a solar panel (Cubas, Pindado, and De Manuel, 2014)

Figure 1.2 shows the I-V and P-V characteristics of a solar cell. The horizontal axis is the voltage of the photovoltaic cell while the vertical axes are the current and power of the cell. V_m, I_m and P_m are the maximum voltage, maximum current and the maximum power of the solar cell respectively. V_{oc} is the open circuit voltage of the solar cell. I_{sc} is the short circuit current of solar cell. The controller of the power electronics converters determines the optimum operating point, which is called as the maximum power point (MPP) according to overall system parameters.

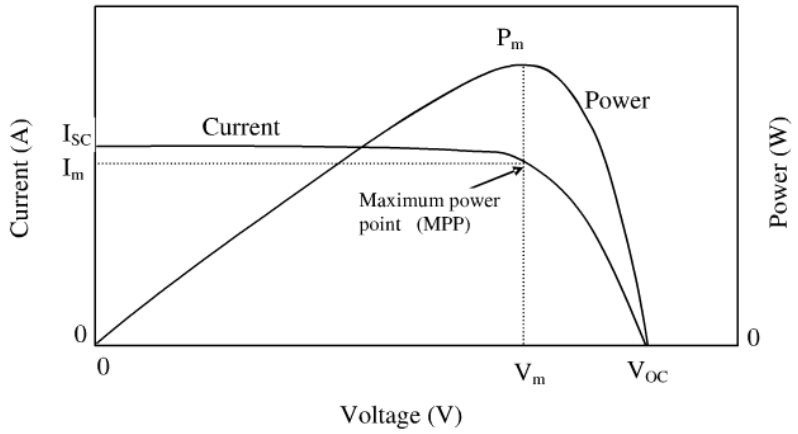

Figure 1.2. I-V and P-V characteristics of solar cell (Mohammed and Devaraj, 2014)

1.3.2. Fuel Cells

In recent years, there has been an increasing interest in fuel cells as the result of their superior features such as modularity, high efficiency, load flexibility and zero emissions (İnci & Türksoy, 2019). A fuel cell is an electromechanical device that converts energy produced from

a chemical reaction directly into electrical energy. Fuel cells usually utilize hydrogen as the fuel, and oxygen as the oxidant in the electrochemical reaction. The hydrogen fuel cell is formed by combining hydrogen and oxygen to produce electricity, with water and heat as its by-product. A fuel cell consists of anode, cathode, electrolyte and external load circuit as demonstrated in Figure 1.3.

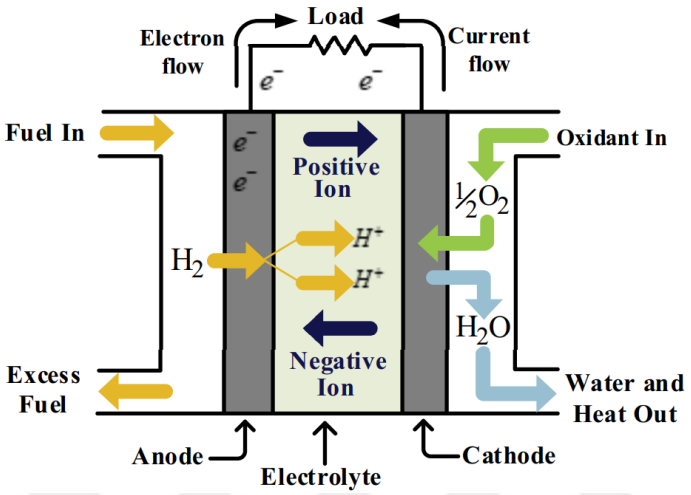

Figure 1.3. Basic structure of fuel cell (İnci and Türksoy, 2019)

There are various types of fuel cells such as solid-oxide FC (SOFC), alkaline FC, direct methanol FC, high temperature proton exchange membrane FC, phosphoric acid FC, and molten carbonate FC. Solid-oxide FCs are the most frequently used FCs as they have high operating life, solid-state construction and high-temperature operation (Minh, 2004). Industry applications of FC are hybrid electrical vehicles, unmanned aerial vehicles, uninterruptible power supplies, and portable electronic devices (Stambouli and Traversa, 2002). The power produced by the FC stack is related to the number of cells, operating temperature, operating pressure, air flow, flow rates of reactants and humidity of reactants (Forrai et al., 2005). The type of fuel cell used in this study is SOFC. SOFCs are high-temperature fuel cells and they use a solid ceramic material as electrolytes. Here, water and heat are produced when oxygen and hydrogen interact. The SOFC generate electricity at a high operating temperature of about 700-1000 ^{o}C. The main advantage of the SOFC's is that they are operated at high efficiency of 50-60% (Kirubakaran, Jain, and Nema, 2009).

1.3.3. Energy Storage Units

Nowadays, energy storage is a significant part of the energy supply chain. ESUs provide a number of benefits, including enhancing grid stability, ensuring bidirectional power flow, and increasing the efficiency. Due to the intermittent nature of RESs, especially solar and wind, energy storage plays a crucial role in hybrid power generation systems in terms of power quality and voltage smoothing. Thus, energy storage technologies have gained increased attention and have become more than a necessity in recent years.

The device that converts electrical energy obtained from power systems into a form that can be stored and converted back to electrical energy when needed is referred to as an energy storage system. Energy storage technologies are categorized as long-term, and short-term according to storage duration. Additionally, they are classified by the kind of storage as electrical, mechanical, chemical, thermal ESUs. The main types of energy storage are:

- Pumped hydro storage
- Compressed air energy storage
- Battery storage systems
- Superconducting magnetic energy storage
- Flywheel energy storage
- Supercapaticor storage systems

Batteries and supercapacitor banks, which are long-term energy storage devices, are the most popular kinds of ESUs. Batteries are rechargeable devices that convert chemical energy to electrical energy and store it inside their structures. The power generated by batteries is associated with many parameters as energy density, cell voltage, charge and discharge currents, cycle life, state of charge and state of health.

Lead-acid, lithium-ion, nickel cadmium, and nickel-metal-hydride batteries are essential battery types. Li-ion batteries which is shown in Figure 1.4, are the most widely used battery type due to the long life cycle, wide operating temperature range, high energy efficiency and fast charging features. The type of battery used in this study is lithium-ion.

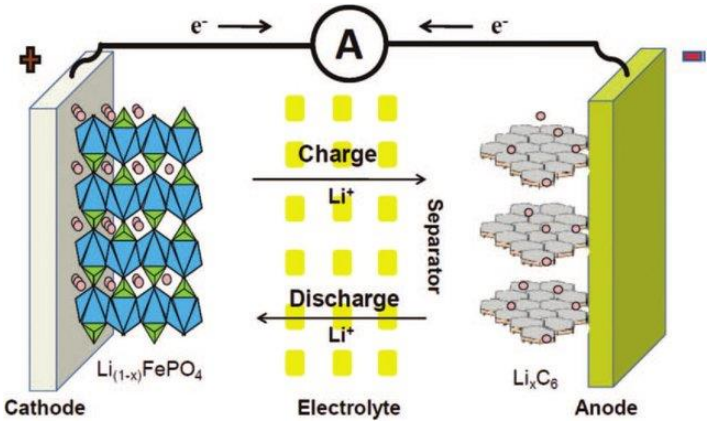

Figure 1.4. Structure of li-ion battery (Lochala et al., 2017)

1.3.4. Concept of Hybrid Power Generation System

The power produced by RESs, especially solar and wind, is uncertain and unpredictable as it is affected by environmental conditions that change naturally during the day. The growing usage of RESs and the intermittent nature of the power provided by them causes challenges in the main electrical grid in terms of stability and power quality. Control of the power and frequency is essential to figure out these issues properly. It is necessary to use energy storage technologies in order to control the power flow by regulating the variability of the generated power (Etxeberria et al., 2010). Consequently, hybrid power generation systems that incorporate ESUs are proposed to overcome the drawbacks that come from the intermittency of RESs. The most widely used application areas of these systems are hybrid electric vehicles and DC microgrids (Savrun and Atay, 2020) (Kolahian et al., 2019). The block diagram of the hybrid power generation system with microgrid is given that in Figure 1.5.

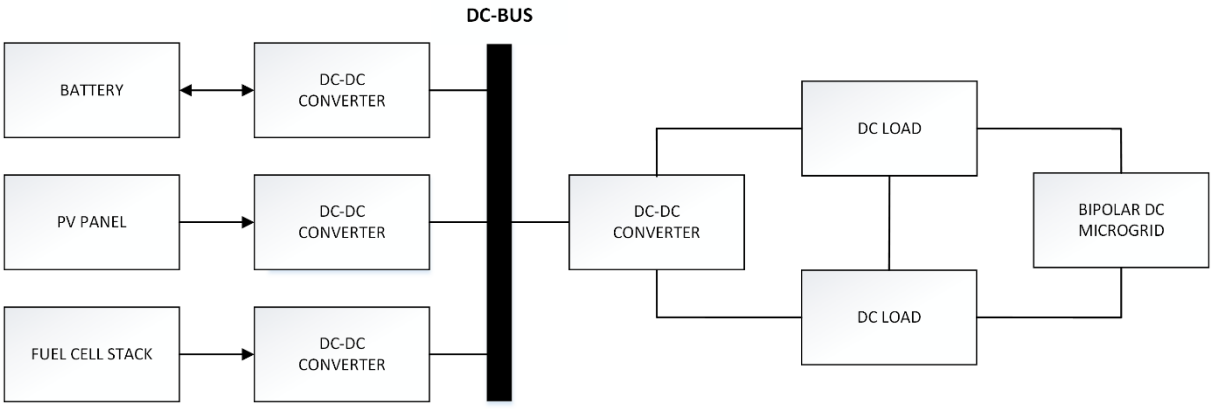

Figure 1.5. Block diagram of hybrid power generation system

1.4. Power Electronics Converters

Power electronics converters have attracted great attention from the past to the present due to their use has become indispensable in many industrial applications. A power electronic device consists of a converter built on a matrix of power semiconductor switching elements and an electronic control circuitry. The converters can be classified as: rectifier (AC-DC converter), inverter (DC-AC converter), chopper (DC-DC converter), AC power controller (AC-AC converter at same frequency), and cycloconverter (AC-AC converter at various frequency). Power converters are often encountered in a wide range of systems such as power generation and distribution, high voltage DC transmission, power quality applications, RESs, uninterruptible power supplies, motor drives, energy storage and electric vehicles. On the other hand, the power converters are used as an interface between the RESs, ESUs and the microgrid. Adopting an independent converter for each connection of source increases both the cost and complexity of the system. MPCs allow the integration of multiple distributed generation resources and loads, providing an effective-cost solution.

1.4.1. DC-DC Converters

DC-DC converters are used to convert the unregulated DC input into a controlled DC output at a desired voltage level. DC-DC converters offer a method of generating multiple controlled voltages from a single battery voltage. The basic block diagram of DC-DC converters is given in Figure 1.6. Nowadays, DC-DC converter models achieve an efficiency of over 90%, using the latest components and control techniques. Basic topologies are usually controlled by pulse width modulation (PWM) method.

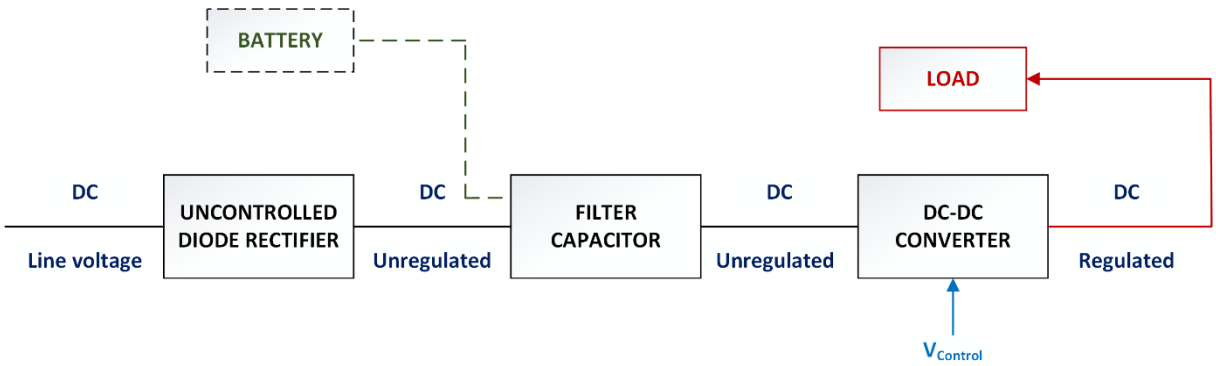

Figure 1.6. Basic block diagram of DC-DC converters

DC-DC converters are commonly used in applications requiring regulated DC power such as: laptop computers, communication devices, medical instrumentation, television receivers, battery chargers and electric vehicles. The main application areas of DC-DC converters are DC motor control, switched power supplies, uninterruptible power supplies, power factor correction, DC welding machines, feeding inverters, DC voltage sources and regulators.

Fundamental topologies of DC-DC converters are examined in two basic categories: transformerless DC-DC converter topologies and transformer based DC-DC converter topologies. Transformerless topologies are as follows: buck (step-down), boost (step-up), buck-boost (step-down/step-up), and cuk converters. Transformer based topologies are flyback, forward, and push-pull converters.

The isolated bidirectional DC-DC converter topology has been widely used with presence of advantages such as buck and boost conversion modes, high frequency operation, bidirectional power flow and galvanic isolation. These converters are commonly used in various power electronics applications such as isolated cuk and single-ended primary-inductor converter (SEPIC)/zeta, push-pull, dual-active bridge, and MPC topologies. To achieve high efficiency power conversion and flexible voltage regulation is a major challenge for design and implementation of high performance bidirectional power converters (Wu et al., 2020). The integration of bidirectional DC-DC converter topologies into DC microgrids has become a popular research topic in recent years.

1.5. Background and Research Motivation

In recent years, the usage and applications of renewable energy have greatly increased due to the environmental problems, depletion of fossil fuels, rapid development of technology, and the growth of the world population. Besides, renewable energy integration into power generation systems, which is among popular research topics, has gained remarkable progress.

DC microgrids, in which renewable energy sources can be integrated more easily than AC microgrids, have become an important alternative to traditional power systems. To improve the efficiency and power quality, bipolar type DC microgrids have been suggested (Kakigano et al., 2010). Even though BPDCMGs are advantageous in terms of high efficiency and power

carrying capacity, power flow management and voltage imbalances between terminals are the issues that need to be investigated (Tavakoli et al., 2016).

In the literature, many MPC topologies have been proposed in order to integrate multiple renewable energy sources and energy storage elements into DC microgrids and to manage them effectively. There are only a few theoretical and simulation studies related to multiport DC-DC converters that have voltage balancing function in BPDCMGs. With the aim of filling aforementioned gap in the literature, this study has been proposed.

In this thesis study, a five port isolated bidirectional DC-DC converter is proposed for interfacing PV/FC/battery systems with BPDCMGs. The proposed topology and its controller is modeled in MATLAB/Simulink environment. The steady-state and dynamic performance of the system has been evaluated by three different case studies. The developed topology come forward with reduced switch number, high efficiency and cost-effectiveness. It can be used for integration of RESs to BPDCMG, power flow management between input/output ports, and compensation of bipolar output voltage differences.

1.6. Objectives of the Thesis

The objectives of this thesis are as follows:

- To describe power system definitions and power generation systems,
- To give information of renewable energy systems, hybrid power generation systems, AC microgrid, DC microgrid and BPDCMG concept,
- To introduce MPCs which are capable of integrating RESs and ESUs to DC microgrids,
- To present literature survey of multiport DC-DC converters with their controllers and power circuit topologies,
- To describe modeling of FPIBC with power circuit configuration and control system,
- To propose voltage balancing function and operation modes of the controller,

- To examine all possible power flow scenarios between the input/output ports,

- To evaluate the performance of the FPIBC with simulation studies,

- To contribute scientific literature by the publications made as a result of this study.

1.7. Outline of the Thesis

Outline of the thesis is organized as follows:

- Chapter 1 introduces power generation systems, types of microgrids, BPDCMGs, renewable energy systems and batteries. Then, general information about power electronics converters and DC-DC converters are presented given.

- In Chapter 2, multiport DC-DC converters are described in detail. A comparison of the proposed topology with other multiport DC-DC converter topologies in the literature is also elaborated.

- In Chapter 3, power circuit configuration, control system, and operation modes of the converter are addressed.

- In Chapter 4, simulation results for three different case studies are presented and the discussions are provided.

- In Chapter 5, significant conclusions and the main contributions of the study are highlighted.

- Finally, related references used in the thesis and biographical information of the author are presented.

2. LITERATURE REVIEW

2.1. Review of Bipolar DC Microgrids and Voltage Balancers

Bipolar type DC microgrids with two voltage levels in a three-wire DC line (positive, negative, and neutral) have been introduced to increase power quality and reliability (Kakigano et al., 2010). BPDCMGs are preferred particularly in data centers, as they can feed critical loads using the other two remaining wires when an abnormal condition or fault occurs in one wire (Ahmadi, Rokrok, and Hamzeh, 2018a). Although BPDCMGs provide advantages in terms of high efficiency and power carrying capacity, voltage differences between the upper and the lower terminals, voltage stability, and power flow management are the issues that need to be investigated (Tavakoli et al., 2016).

The voltage imbalance is one of the crucial concerns encountered in BPDCMGs that several studies have been addressed to mitigate their adverse effects on power quality. In order to acquire symmetrical bipolar output voltages, series-connected power converters or voltage balancers are proposed in the literature.

A bidirectional dual buck-boost voltage balancer with direct coupling as shown in Figure 2.1 is put forward to keep output voltage balanced in a low-voltage bipolar type DC microgrids. A novel burst-mode control technique for the dual buck-boost voltage balancer was developed to improve system efficiency and reliability. Under the burst-mode control scheme, the basic operating principle and a small-signal model of the voltage balancer were examined. Simulation and experimental results showed that the bidirectional dual buck-boost voltage balancer can balance output voltages with unbalanced AC/DC loads (Liu et al., 2015).

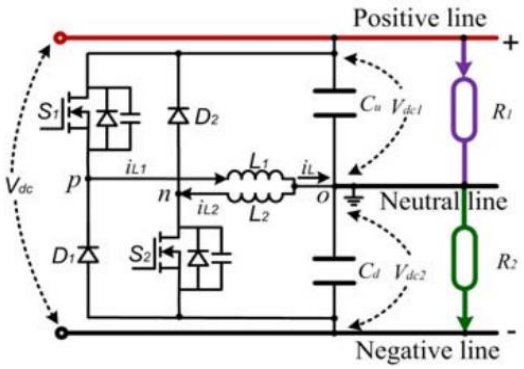

Figure 2.1. Bidirectional dual buck-boost voltage balancer (Liu et al., 2015)

Two types of voltage balancing circuits, namely simple type and converter type, and control strategies for DC distribution were investigated (see in Figure 2.2. and Figure 2.3.). The simple type voltage balancer's simulation results demonstrated that both AC and DC power can be supplied simultaneously and reliably. The voltage balancing control and the power flow management were performed concurrently, according to the simulation results of the DC-DC converter type voltage balancer (Kakigano et al., 2007).

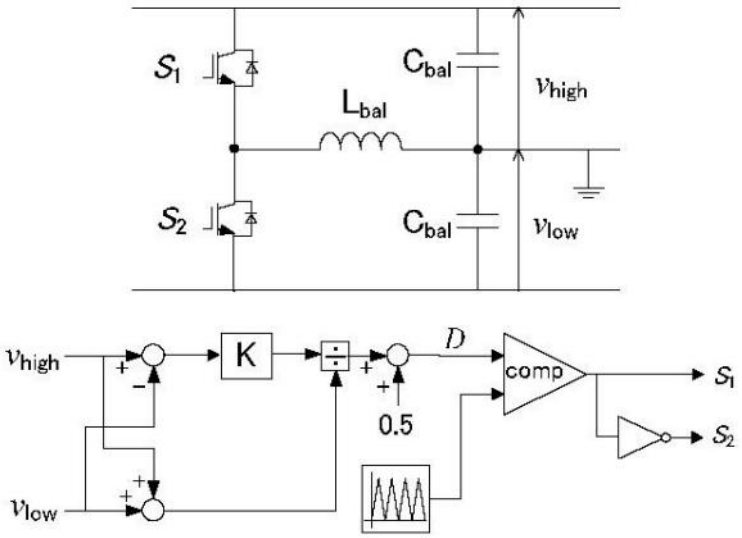

Figure 2.2. Circuit and control scheme of simple voltage balancer (Kakigano et al., 2007)

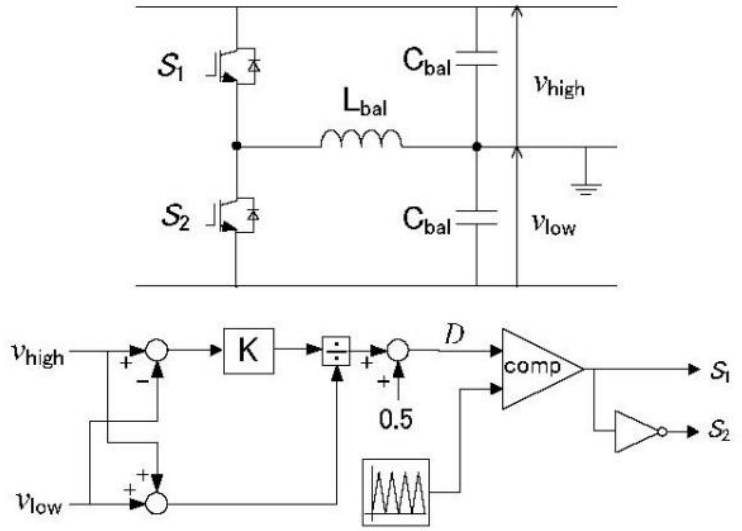

Figure 2.3. Circuit and control scheme of the converter type voltage balancer (Kakigano et al., 2007)

A voltage balancing circuit based on a neutral point clamped converter (see in Figure 2.4.), operated only when the system is driven out of the balanced zone, was introduced. The balancing concept allowed reduced switch stress, inductor size reduction, and usage of higher switching frequencies. The distributed DC bus structure provided the system with a reduced number of power conversion stages, lower costs and increased overall efficiency. Fast charging for plug-in electric vehicles was possible with the suggested architecture, which concentrates many charging units into a central grid-tied converter. Furthermore, it permitted the integration of PV generation with energy storage systems, allowing the chargers' power demand to be reduced while providing support to the grid (Rivera et al., 2015).

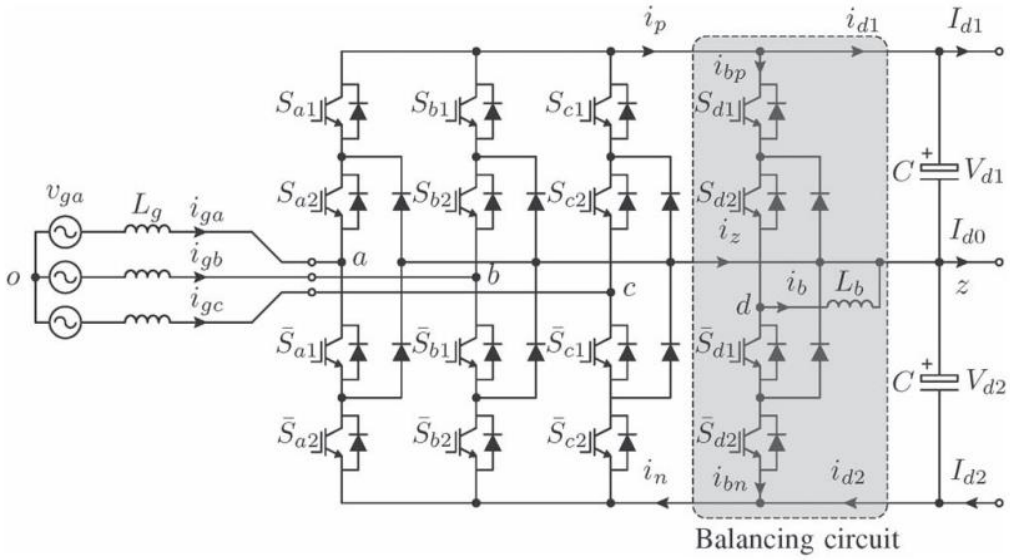

Figure 2.4. Grid-tied three-phase neutral point clamped converter with a balancing leg (Rivera et al., 2015)

Based on the operating principle of an existing buck-boost type voltage balancer, a deduction approach for a series of voltage balancers was offered. Different types of converters such as interleaved buck-boost, cuk, super-SEPIC, and super-zeta were employed as voltage balancers. Interleaved buck-boost type voltage balancer was selected as an example for experimental validation. Results showed that buck-boost topology has a promising capability of voltage balancing between two DC buses (Wang et al., 2017).

A novel single-input dual-output, boost-SEPIC type interleaved DC-DC converter was presented and used for mitigation of the voltage imbalance in a low-voltage BPDCMG. This converter improved efficiency with the help of ensuring zero voltage switching (ZVS) turn-on

and turn-off of the complementary metal oxide semiconductor field effect transistors (MOSFETs). Another notable characteristic was the absence of an active source to mitigate the voltage imbalance. Furthermore, it was observed that reduction of the ripple in the input current is provided due to the interleaved structure of the presented converter (Prabhakaran & Agarwal, 2020).

A three-port multi-directional DC-DC converter with a burst-mode control strategy was developed and presented for both integrating a battery system to a BPDCMG and compensating voltage imbalances (see in Figure 2.5.) (Ahmadi, Rokrok, and Hamzeh, 2018b), (Ahmadi et al., 2018a). In order to examine the stability of the system, a small-signal model was evolved. The suggested converter's ability to balance bus voltages with unbalanced loads was illustrated through simulation and experimental results. It was obtained that, this three-port multidirectional converter's construction enhanced system efficiency by the fact that it can be used instead of several independent converters and due to its multi-mode operation (Ahmadi et al., 2018a).

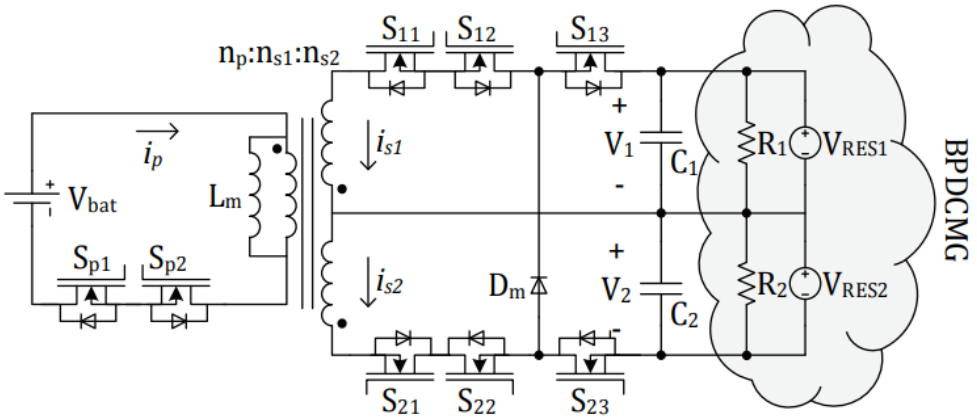

Figure 2.5. Three-port multidirectional converter for integrating a battery system to a BPDCMG (Ahmadi et al., 2018b)

To obtain symmetrical or asymmetrical bipolar DC output, the dual active half-bridge topology was used (see in Figure 2.6.). A control method combining duty-cycle and phase-shift control was proposed, followed by an examination of various operating conditions. Thus, voltage balancing functionality was provided without the need for additional circuitry (Gao and Rogers, 2018).

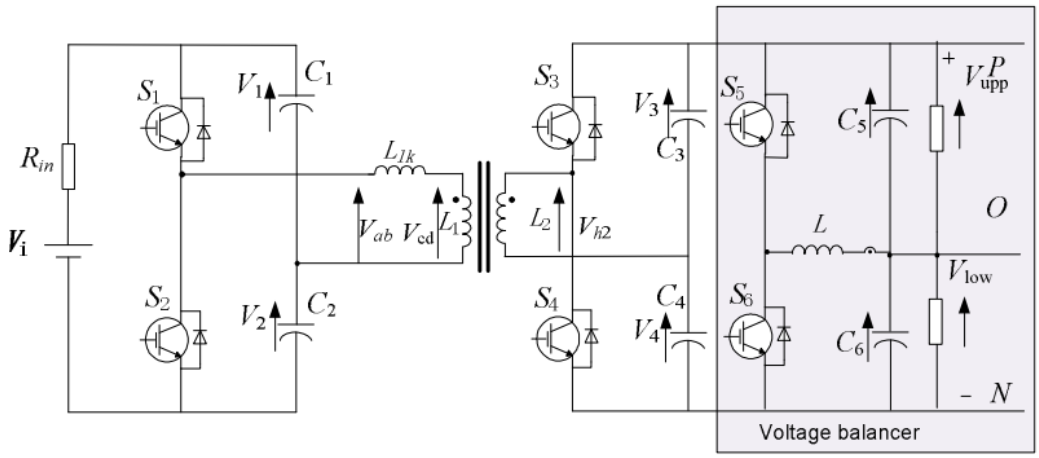

Figure 2.6. Dual active half bridge with voltage balancer (Gao and Rogers, 2018)

2.2. Review of Multiport DC-DC Converters

MPCs are being developed and their use is becoming increasingly common, with the aim of reducing the number of converters and providing integration between the source and load sides. There is a number of features that MPCs are advantageous when compared to conventional two-port converters such as ease of integration with RESs and ESUs, reducing the number of switches, improving efficiency and power quality.

A comparison between two main architectures of high-voltage DC-DC converters for power distribution systems of the modern aerial vehicle's has been made, then MPCs and conventional two-port converters are reviewed (Swaminathan and Cao, 2020). The classification of DC-DC power converters can be summarized as shown in Figure 2.7.

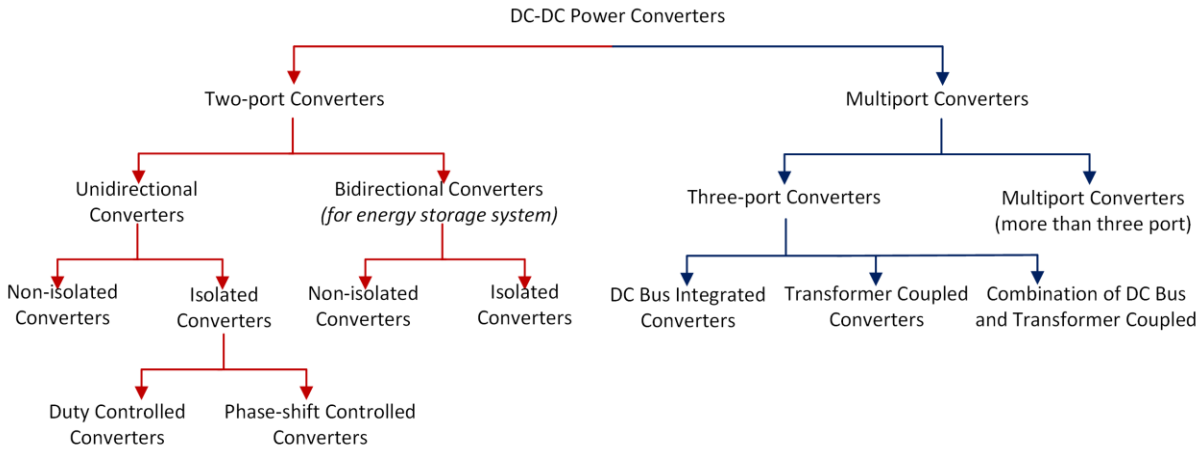

Figure 2.7. The classification of DC-DC power converters (Swaminathan and Cao, 2020)

It has been reported that multiport DC-DC converter structures are classified into two fundamental categories as non-isolated and isolated (Askarian et al., 2021) (Mohseni et al., 2019). The non-isolated MPCs derived from the buck, boost, and buck-boost converters have advantages of more compact design and high power density (Savrun and Atay, 2020). These types of MPCs are more suitable for low voltage DC microgrid applications as they are less reliable due to the lack of high-frequency transformer (HFT) (Prabhakaran and Agarwal, 2020), (Zhang, Sutanto, and Muttaqi, 2016). There have been various four-port non-isolated converter topologies are presented for interfacing hybrid RESs and ESUs to BPDCMGs (Tian et al., 2020) (Prabhakaran and Agarwal, 2020).

A dual-input dual-output DC-DC converter was presented, which is employed for interfacing FC and PV resources to a low-voltage BPDCMG system. Dynamic modeling of the converter was analyzed considering the different duty ratio conditions. Simulation results for both open-loop and closed-loop controller demonstrated that the converter achieve maximum power point tracking (MPPT) operation of PV under varying conditions such as solar irradiation and load power demand (Prabhakaran and Agarwal, 2020).

A four-port non-isolated converter that combined from SEPIC three-port converter and cuk three-port converter was designed (see in Figure 2.8). The presented converter was used for interfacing the PV-battery system and for obtaining symmetrical bipolar output. It was specified that the effectiveness of the proposed converter was verified by experimental results under steady-state and dynamic response (Tian et al., 2020).

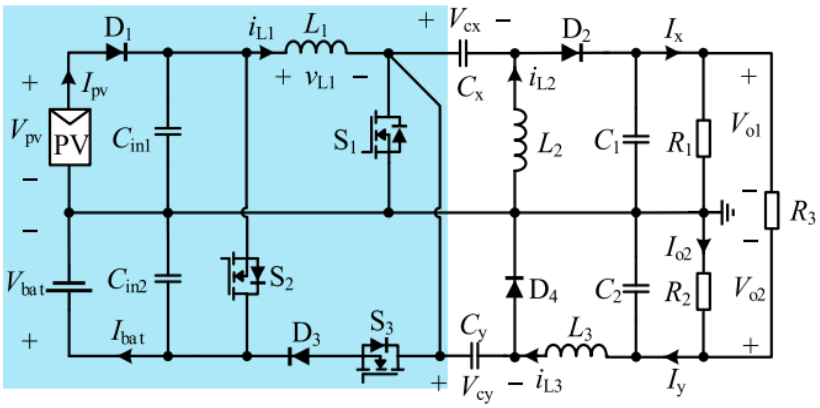

Figure 2.8. Four-port non-isolated converter for interfacing PV-battery system (Tian et al., 2020)

A non-isolated three-port multidirectional converter based on a buck-boost converter was proposed to perform battery management and voltage balancing features in a BPDCMG. It was stated that the system efficiency was improved due to the absence of many separate converters (see in Figure 2.9.) (Ahmadi, 2020).

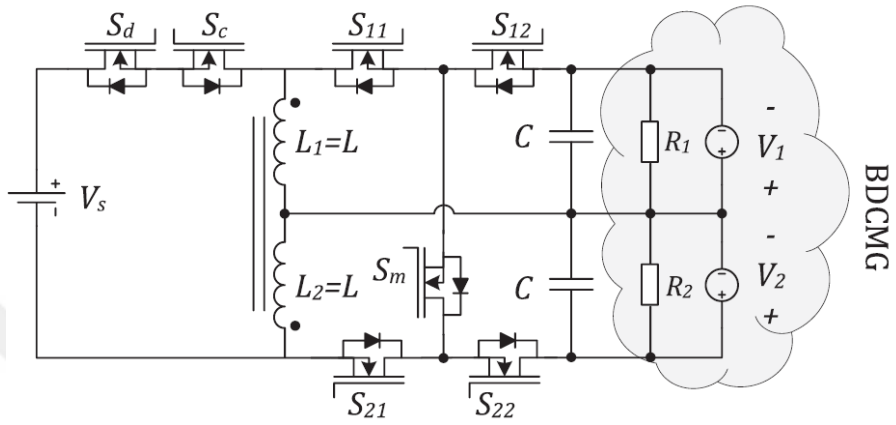

Figure 2.9. Three-port multidirectional buck-boost converter (Ahmadi, 2020)

The isolated MPCs, commonly formed from half-bridge or full-bridge topologies, are utilized in medium voltage DC microgrids for critical applications that require isolation. These type of MPCs excels with providing galvanic isolation and more flexible voltage levels by using HFT, and easier implementation of soft switching (Kolahian et al., 2019). On the other hand, a large number of research studies have been carried out on the isolated MPCs that have disposed to bidirectional power transfer, isolation, and soft switching (Savrun et al., 2020).

An isolated soft-switched three-port converter basis on the interleaved full-bridge topology with pulse width modulation and phase-shift control was developed to control power flow between RESs. Duty-cycle control was employed to regulate the output voltage at this system (see in Figure 2.10.). The experimental results revealed that the power flow across the three ports can be effectively regulated using the two decoupled control variables (Mira et al., 2017).

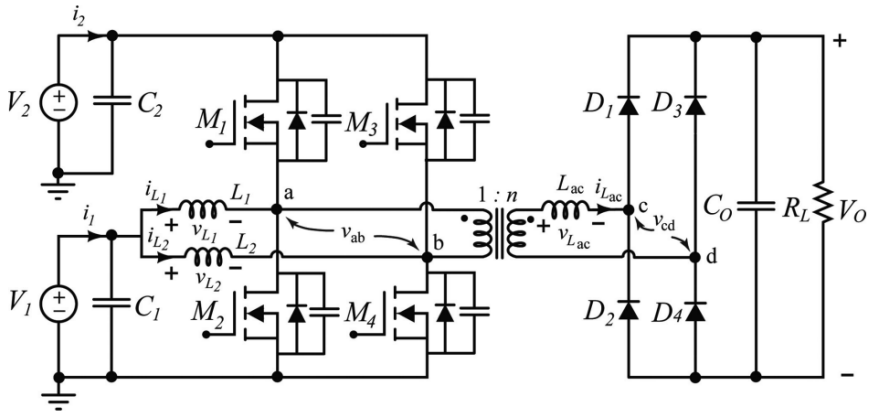

Figure 2.10. Three-port converter for hybrid renewable energy systems (Mira et al., 2017)

An interleaved half-bridge MPC was presented for a renewable power system (see in Figure 2.11). This system was utilized for interfacing three ports: a bidirectional battery unit port, a source port, and an isolated load port. PWM and phase-shift control were adopted to regulate the power transfer between the ports. Besides, ZVS was implemented to primary-side switches to reduce the switching losses in this system. The effectiveness of the suggested converter was verified by experimental results on a 500-W prototype (Wu et al., 2016).

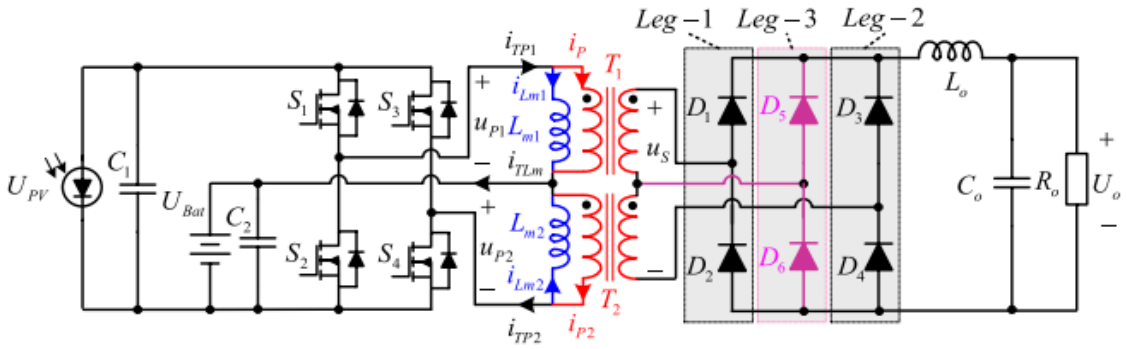

Figure 2.11. Interleaved half-bridge three-port converter (Wu et al., 2016)

An isolated multiport DC-DC converter, which is the combination of interleaved bidirectional topology on the primary side and neutral point clamp on the secondary side, was developed for BPDCMG applications (see in Figure 2.12.). The proposed converter was experimentally applied to a hybrid generation system consisting of PV, FC, and battery. In addition, the proposed converter was simulated in the MATLAB/Simulink software environment in several power-sharing modes (Kolahian et al., 2019).

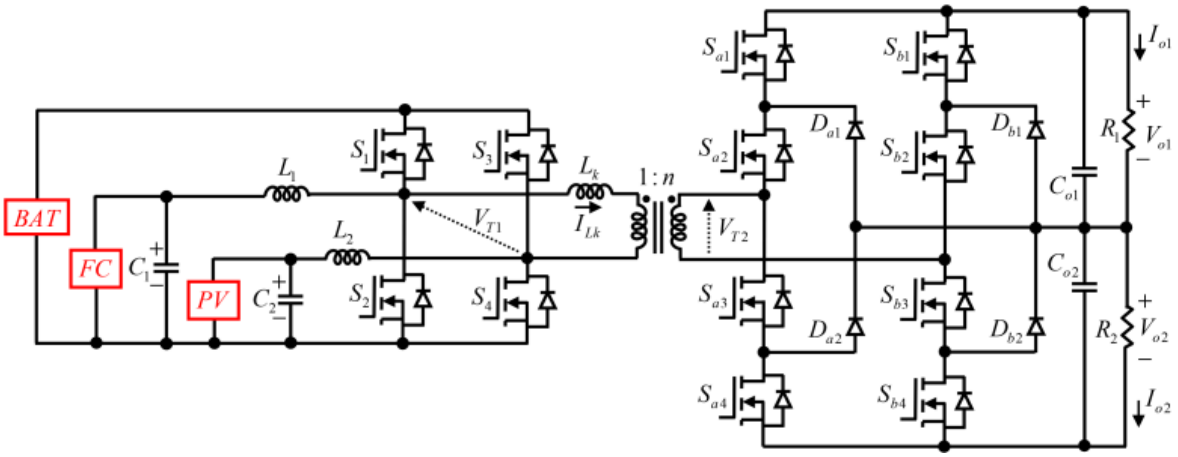

Figure 2.12. Multiport bipolar DC-DC converter (Kolahian et al., 2019)

A high-gain bidirectional three-port converter topology capable of interfacing low-voltage supercapacitor-battery based hybrid energy storage systems into a DC microgrid was introduced (Chaudhury and Kastha, 2020). In that topology, a current-fed dual active bridge is utilized to provide galvanic isolation of the battery from the DC bus, a wide ZVS range for all switches, and bidirectional power flow between the ports. On a 1-kW laboratory prototype, the effectiveness of the proposed topology and control technique were tested. It was observed that the developed prototype achieves a peak efficiency of 95.96% which is higher than existing MPCs.

A study was conducted on isolated four-port converter based on center-tapped winding to integrate RES and ESS to bipolar DC buses. The performance of the converter was validated in terms of power and voltage relationship, port current ripple, soft switching and control method experimentally by a 500-W prototype. It was highlighted that the proposed converter is suitable for applications with low output voltage levels because of high voltage stress on switches (Tian et al., 2022).

Pires et al. (2021), presented and analyzed a topology of DC-DC converter which has bipolar output, high voltage gain, and continuous input current. The performance of the converter was validated through the experimental results. It was specified that the proposed structure was suited for bipolar DC microgrids or transformerless grid-tied PV and FC resources because of the self-balancing bipolar outputs.

A multiport converter based on LLC resonant converter was introduced. This converter consists of three ports as an input port, a battery port, and a load port. Methods of pulse-frequency modulation and phase-shift control were applied to this topology. Thus, the input power and output voltage can be adjusted separately. In addition, it was stated that the presented topology can be used in DC grid applications (Zhang et al., 2019).

An isolated bidirectional multiport DC-DC converter that makes use of a lower count of switches in comparison with other topologies explained (see in Figure 2.13.) (Zeng, Qiao, and Qu, 2015). The presented converter had the capability of simultaneous power management between multiple RESs as a PV, a rechargeable battery, and a load.

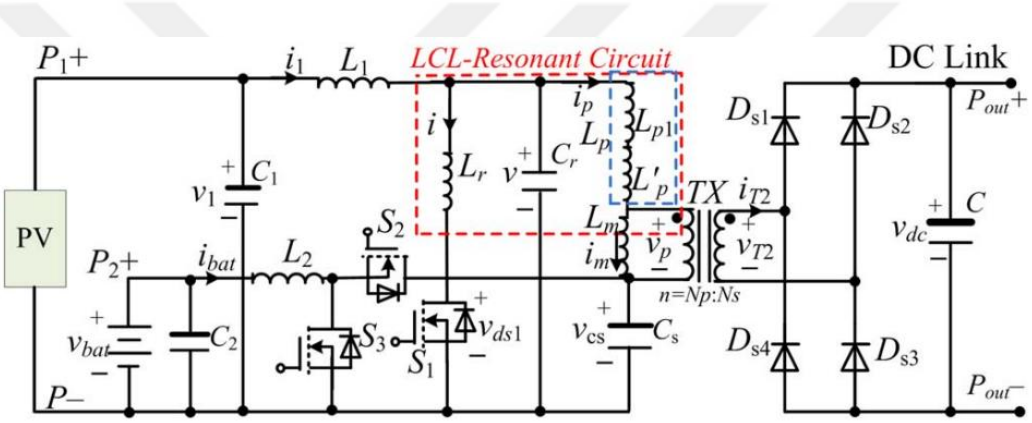

Figure 2.13. Isolated three-port bidirectional DC-DC converter for a PV and battery system (Zeng et al., 2015)

An isolated bidirectional multiport DC-DC converter topology which one port connected to the DC bus for hybrid energy applications with supercapacitor and battery was presented. From the experimental results, it was observed that this topology provided ZVS, low input current ripple and bidirectional power flow between ports for all switches (Ding et al., 2014).

An isolated multiport DC-DC converter utilizing a reduced number of switches was offered for simultaneous power management of multiple RESs. This converter was applied to a three-source hybrid generation system that includes wind and solar energy (see in Figure 2.14.). Experimental results were presented to demonstrate the effectiveness of the proposed converter (Jianwu et al., 2014).

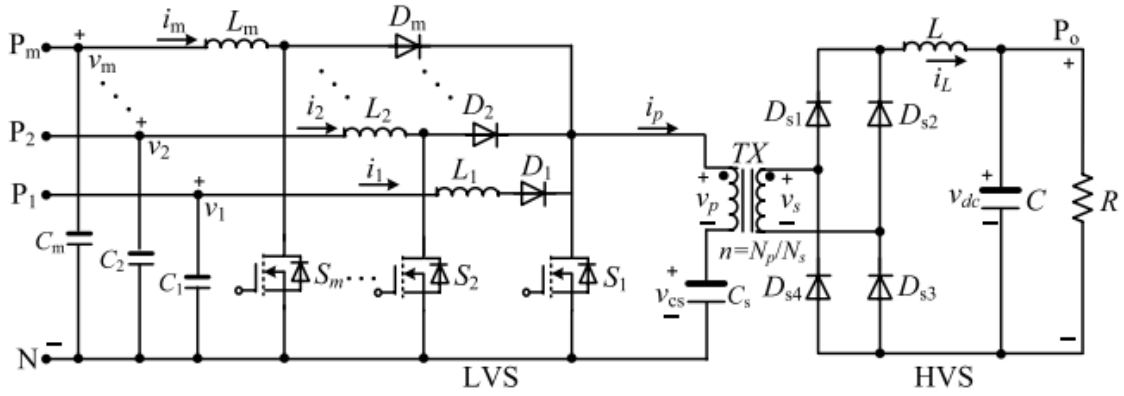

Figure 2.14. Topology of the isolated multiport DC-DC converter (Jianwu et al., 2014)

A four-port isolated bidirectional DC-DC converter that integrates a PV panel, a wind turbine and a battery unit to a DC microgrid was put forward. Due to the integrated structure and soft switching, it was concluded that 95% peak efficiency was achieved at approximately 50% rated load in both buck and boost modes. Experimental results of steady-state analysis validated that the offered structure ensured ZVS conditions and associated power relationships while maintaining high efficiency (Zeng, Du, and Yang, 2021).

A five-port converter that can interface PV modules and battery with DC microgrid was proposed and it was indicated that this converter had three ports as one port for DC microgrid and one port for battery. Experimental and simulation studies were carried out to verify the performance of the proposed converter. It was stated that as a prominent feature, it was ensured that all PV modules are operated on their MPPs (Vettuparambil, Chatterjee, and Fernandes, 2021).

A reduced switch topology and control mechanism for a quasi-Z-source converter integrated isolated multiport bidirectional DC-DC converter was proposed. It was understood from the simulation results that the proposed system performed all power flow changes between the ports and enforced a control mechanism consisting of constant current/constant voltage charge for battery, MPPT for PV and DC-link control (Savrun and Atay, 2020).

A PV port isolated three-port DC-DC converter derived from the half-bridge topology was developed for simultaneous connection of a PV port, a battery port, and a load port. A 500-W prototype was designed and tested, the experimental results demonstrated that the validity of

this proposed converter, exhibiting high dynamic response and low output impedance (Zhu et al., 2015).

A dual active bridge MPC was addressed to interface two PV modules and a battery with a 380 V DC microgrid. It was emphasized that, depending on the atmospheric conditions, these two solar PV modules can be operated at their MPPs. High voltage gain between the DC microgrid, PV and battery ports was obtained by employing an HFT. Moreover, an optimization method to minimize the transformer current at this system was presented. The performance of the MPC was verified by conducting experimental studies on the developed 1 kW prototype (Vettuparambil, Chatterjee, and Fernandes, 2022).

There have been numerous research studies conducted on multiport DC-DC converters for interfacing RESs and ESUs with BPDCMGs in the literature. It is seen that among these studies voltage balancing in BPDCMGs is not investigated in detail. However, it is known that the voltage balancing is an important issue for the power quality in BPDCMGs.

2.3. Comparison of the Proposed Topology with Other Multiport DC-DC Converters

In this thesis, a new five-port isolated bidirectional DC-DC converter topology is proposed to compensate the voltage imbalances in BPDCMGs. A comparison of the proposed topology with similar multiport DC-DC converter topologies in the literature is tabulated and detailed. Table 2.1 shows the comparison of the proposed topology with other similar multiport DC-DC converters according to isolation, bipolar output, power flow direction, number of ports, number of switches and diodes, maximum efficiency values.

It can be seen that the proposed topology utilizes fewer switches as compared to (Chaudhury & Kastha, 2020) and (Prabhakaran and Agarwal, 2020), hence reduces the cost of the system. The suggested converter differs from existing topologies in that it contains a bipolar output and a bidirectional battery port. In the proposed topology, higher efficiency values have been achieved compared to the other topologies. It is also more preferable because it contains more port connections according to other topologies.

Table 2.1. Comparison of the proposed topology with other multiport DC-DC converters

Topology	Isolation	Bipolar Output	Power Flow	Number of Ports	Number of Circuit Elements		Maximum Efficiency
					Switch	Diode	
(Prabhakaran and Agarwal, 2020)	No	Yes	Unidirectional	4	2	4	93.00 %
(Ahmadi, 2020)	No	Yes	Unidirectional	3	7	-	NA*
(Tian et al., 2020)	No	Yes	Bidirectional	4	3	4	95.80 %
(Ahmadi et al., 2018b)	Yes	Yes	Unidirectional	3	8	1	~95.50 %
(Ahmadi et al., 2018a)	Yes	Yes	Bidirectional	3	8	1	90.20 %
(Wu et al., 2016)	Yes	No	Bidirectional	3	4	6	94.50 %
(Chaudhury & Kastha, 2020)	Yes	No	Bidirectional	3	10	-	95.96 %
(Zeng et al., 2015)	Yes	No	Bidirectional	3	3	4	94.50 %
(Zeng et al., 2021)	Yes	No	Bidirectional	4	6	2	95.00 %
(Ding et al., 2014)	Yes	No	Bidirectional	3	8	-	NA*
(Kolahian et al., 2019)	Yes	Yes	Bidirectional	5	12	4	94.70 %
Proposed	Yes	Yes	Bidirectional	5	9	4	94.85 %

*NA: Not Available.

2.4. Summary

In this section of the thesis, a comprehensive review of the studies on voltage balancing in BPDCMGs and multiport DC-DC converter topologies which are used for interfacing RESs and ESUs are elaborated in terms of power circuit configurations and control schemes. It is outlined from the literature survey that many academic studies are carried out by considering the advantages of MPCs and by using different modulation and control techniques on the topologies. It is seen that experimental analyses and simulation techniques were used.

It is aimed to contribute to the literature by adding novel five-port isolated bidirectional DC-DC converter topology which is expected to attract the attention of researchers as an alternative to traditional multiport DC-DC converter topologies. The proposed topology stands out with its features listed below:

i. The proposed topology enables the integration of various RESs and ESUs into the BPDCMG.

ii. The suggested topology provides the reducing number of switching devices according to similar multiport DC-DC converter topologies, thus the cost will be reduced at the applications. Besides, less number of switching devices used in the converter ensures increasing the overall efficiency.

iii. Compensation of bipolar output voltage imbalances.

iv. Providing the isolation between input and output ports by HFT.

v. Allows bidirectional power conversion by charging/discharging the battery.

vi. Performing all possible power flow scenarios between the input/output ports.

The viability and effectiveness of the proposed system are demonstrated and validated by simulation results obtained from MATLAB/Simulink.

3. MODELING OF FPIBC

3.1. Power Circuit Design of FPIBC

In this thesis study, a novel isolated bidirectional multiport DC-DC converter topology capable of power balancing up to 500 W imbalance is presented. The main purpose of this structure is to achieve integration of RESs to BPDCMG and to provide bidirectional energy conversion by charging/discharging the battery. Besides, the proposed converter has the ability to compensate bipolar output voltage imbalance conditions.

The proposed FPIBC topology, which consists of two full-bridge converters, a resonant tank, and a voltage balancer circuit, is illustrated in Figure 3.1. In the proposed structure, hybrid generation sources composed of a PV, an FC, and a battery are used for the input ports. On the primary side, FC and PV systems are connected to the full-bridge converter via inductors L_1 and L_2, respectively, while no such inductor is employed to connect the ESU to the circuit. Connection via inductors provides boost characteristics on FC and PV output voltages. The galvanic isolation between the input and output ports is achieved by using an HFT with a unity turns ratio (n=1).

On the secondary side, a circuit structure that composition of voltage balancer circuit and full-bridge converter is used. The voltage balancer circuit comprised from a fully controlled power switch (Q_5) and four diodes (D_x, D_y, D_z, and D_t) is utilized to mitigate the adverse effects of imbalances that occurred in the output voltages on the secondary side. The full-bridge converter generates a bipolar DC voltage, while the voltage balancing circuit makes it possible to compensate for bipolar DC microgrid voltage differences. Furthermore, the proposed topology allows bidirectional power transmission by charging-discharging the battery. In the case where FC and PV charge the battery, there is also a bidirectional power flow between the input ports. On the other hand, the resonant tank reduces switching losses as a result of ZVS operation and ensures that the proposed FPIBC system can achieve high-efficiency values. The series resonant inductor L_{sr}, which includes the leakage inductance of the HFT, and the series resonant capacitor C_{sr} are inserted at the output of the full-bridge converter on the primary side.

As it can be seen from Figure 3.1, V_{dc}, V_{upp} and V_{bot} are the DC voltages, D_x, D_y, D_z and D_t are the diodes, S_1-S_4; Q_1-Q_5 are the main switching elements and n is the transformer turn ratio respectively.

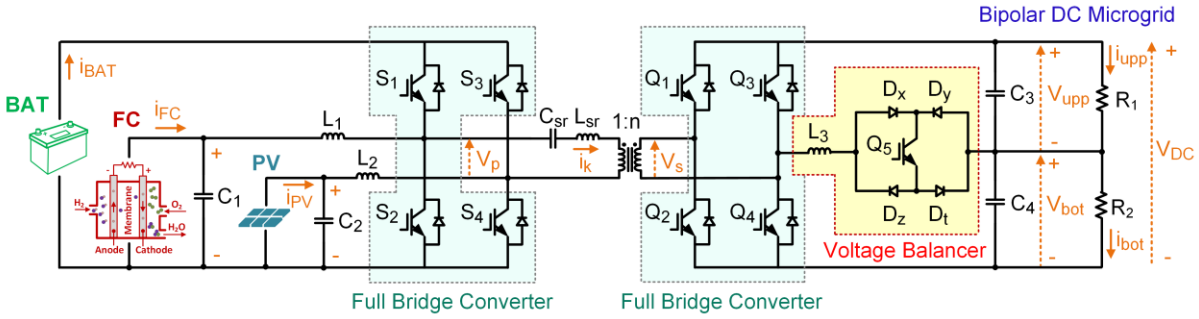

Figure 3.1. Power circuit diagram of the proposed isolated multiport converter

The proposed topology enables power transfer between PV, FC, battery and load. Bidirectional power flow is assured at the battery port by charging/discharging the battery depending on the load demand and the available powers of PV and FC. Considering the equivalent circuits given in Figure 3.3 and Figure 3.5, it appears that there is a boost converter relationship between the PV-battery and the FC-battery respectively.

The basic structure of the boost converter is given in Figure 3.2. The circuit consists of a voltage source, a switching device, diode, inductor, capacitor and a load resistance.

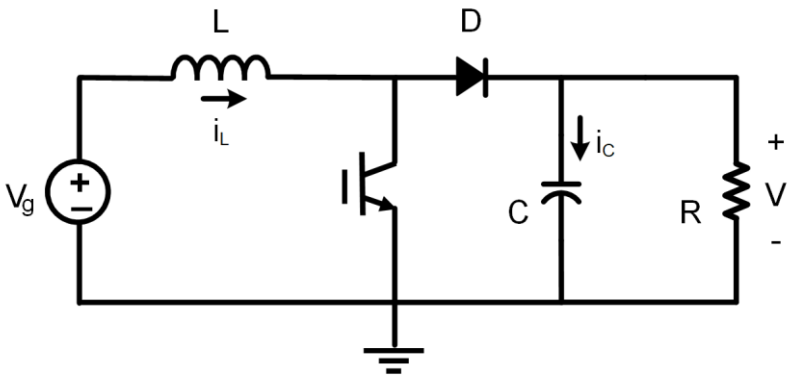

Figure 3.2. Basic structure of boost converter

The controller scheme of the circuit shown in Figure 3.2 is carried out according to the turn- on and turn-off of the semiconductor power switch. When the switch is turned on, the current

passing through the coil increases and energy begins to be stored on the coil. As soon as the switch is turned off, the charging current passing through the coil starts to flow through the diode towards the capacitor and the load. The coil discharges its energy and the polarity of the voltage on the coil becomes the same as the polarity of the voltage source and is connected to the load via the diode. Thus, the level of the output voltage is increased.

Boost converter regulates the output voltage by adjusting the duty cycle (D) value of the related switch. The voltage gain of the boost converter defined as the ratio of the output voltage to the input voltage between the source and load voltages is computed by using Equation 1. When designing a boost converter, Equation 2 and Equation 3 are used to determine required capacitor and inductor values. The desired ripple magnitude in the output voltage (ΔV_c) is calculated and obtained by Equation 2 and the desired ripple magnitude in the input current (ΔI_L) is computed by Equation 3. T_s represents the switching period of the boost converter.

$$\frac{V}{V_g} = \frac{1}{(1-D)} \tag{1}$$

$$\Delta V_c = \frac{V}{RC}.DT_S \tag{2}$$

$$\Delta I_L = \frac{V_g}{L}.DT_S \tag{3}$$

In the proposed topology, the full-bridge converter which interfacing the battery, PV and FC using the switches S_1 and S_2 for PV-battery boost converter while S_3 and S_4 for FC-battery boost converter. S_1, S_2 and S_3, S_4 are pairs of complementary switches on the primary side. The boost conversion between the PV and the battery is realized by using the boost inductor (L_2), the active switch (S_2), the diode of the S_1 switch, and the filtering capacitor (C_2) as highlighted in Figure 3.3. Besides, Figure 3.4 shows the equivalent circuit of boost converter between the PV and the battery.

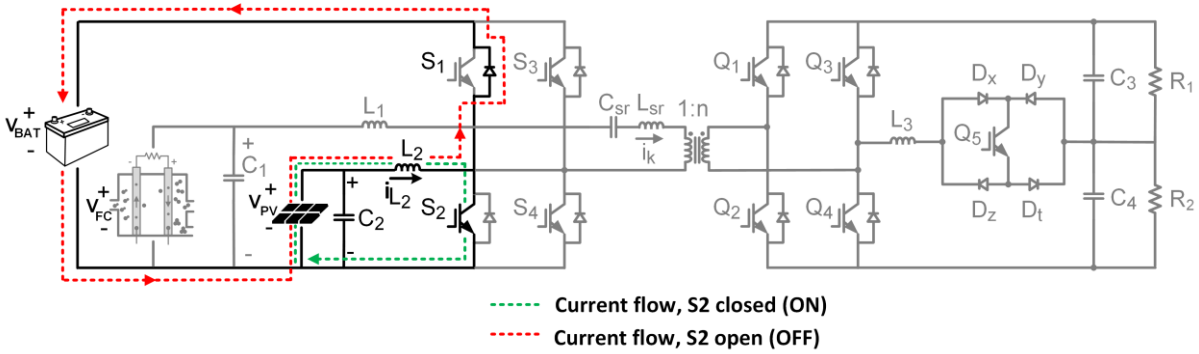

Figure 3.3. Boost converter circuit between PV and battery

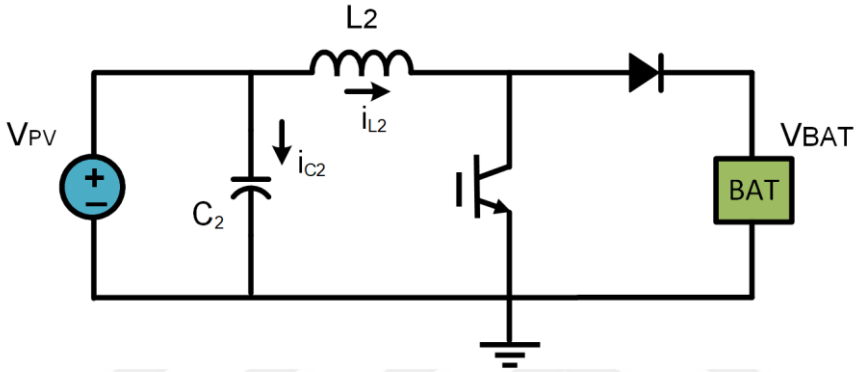

Figure 3.4. Equivalent circuit of the boost converter between PV and battery

The voltage gain of the boost converter between PV and battery is derived by the following equation as emphasized in Figure 3.4;

$$\frac{V_{bat}}{V_{pv}} = \frac{1}{(1-d_{pv})} \tag{4}$$

where V_{pv} and V_{bat} are the PV and the battery voltages respectively. "d_{pv}" defines the duty cycle of the related primary side switches (S_2, S_4).

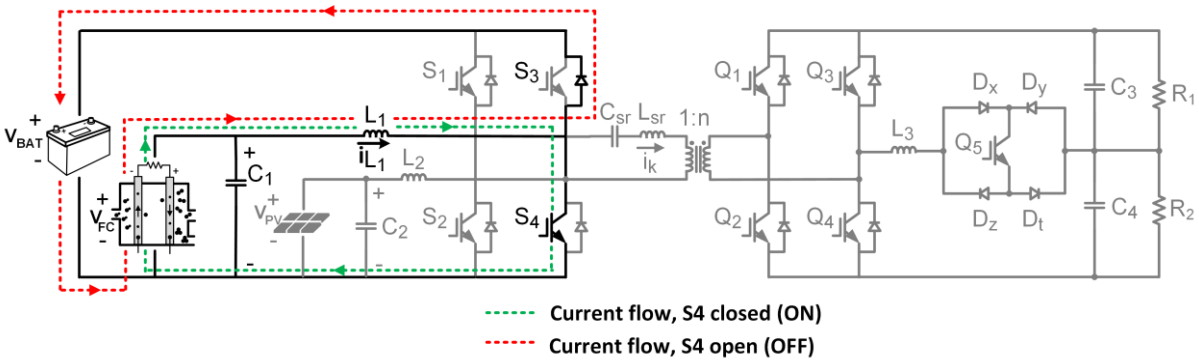

Figure 3.5. Boost converter circuit between FC and battery

Similarly, the boost conversion between the FC and the battery is performed with the inductor L_1, the active switch S_4, the diode of the S_3, and the filtering capacitor (C_1) as shown in Figure 3.5. Figure 3.6 illustrates the equivalent circuit of the boost converter between FC and battery. The voltage gain of this converter is computed by the Equation 5.

$$\frac{V_{bat}}{V_{fc}} = \frac{1}{(1-d_{fc})} \tag{5}$$

where V_{fv} and V_{bat} are the FC and the battery voltages respectively. "d_{fc}" indicates the duty cycle of the related primary side switches (S_1, S_3).

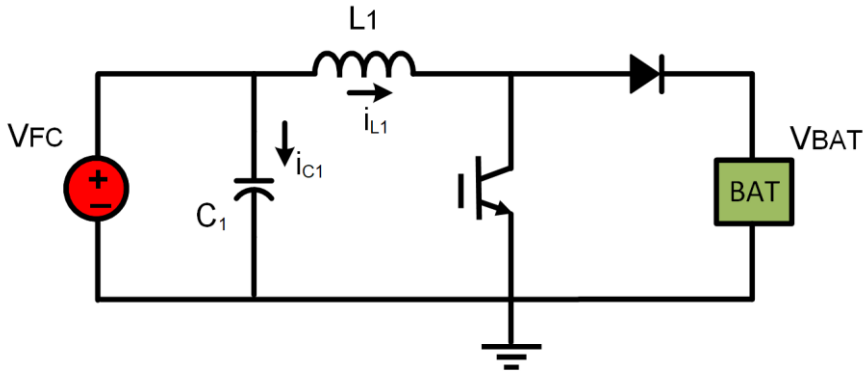

Figure 3.6. Equivalent circuit of the boost converter between FC and battery

The values of boost inductors L_1 and L_2 can be calculated on the basis of the maximum allowed peak to peak ripple currents (Δi_{L1} and Δi_{L2}) and the switching frequency (f_s) as shown in Equation 6 and Equation 7 respectively. The RMS values of voltages of L_1 (V_{L1}) and L_2 (V_{L2}) are expressed in Equation 8 and Equation 9.

$$L_1 = \frac{V_{fc}}{\Delta i_{L1} f_s} d_{fc} \tag{6}$$

$$L_2 = \frac{V_{pv}}{\Delta i_{L2} f_s} d_{pv} \tag{7}$$

$$V_{L1rms} = \sqrt{d_{fc} V_{fc}^{\ 2} + \left(1 - d_{fc}\right)\left(V_{bat} - V_{fc}\right)^2} \tag{8}$$

$$V_{L2rms} = \sqrt{d_{pv} V_{pv}^{\ 2} + \left(1 - d_{pv}\right)\left(V_{bat} - V_{pv}\right)^2} \tag{9}$$

Another structure of the proposed topology is the resonant tank. Equivalent circuit model of the resonant tank is given as shown in Figure 3.7. Resonant converters containing a network of inductors and capacitors called a "resonant tank" are used to reduce switching losses drastically with ZVS and zero current switching (ZCS) capabilities. There are many approaches for the control of resonant converters, the most commonly used method is the frequency control technique (Gücin, Biberoğlu, and Fincan 2019). In frequency control method, efficiency drop occurs due to the sharp changes in switching frequency and the control/design is complicated since the switching frequency varies in a wide range (Alonso et al. 2012). In order to avoid these disadvantages, the phase shift modulation technique with fixed frequency operation is employed.

In this study, a series resonant tank is connected on the primary side of the proposed converter and the system is operated with a switching frequency that is selected higher than the resonant frequency of the tank. The switching losses on the primary side of the proposed FPIBC are reduced owing to the series-connected resonant tank, and thus high efficiency is ensured.

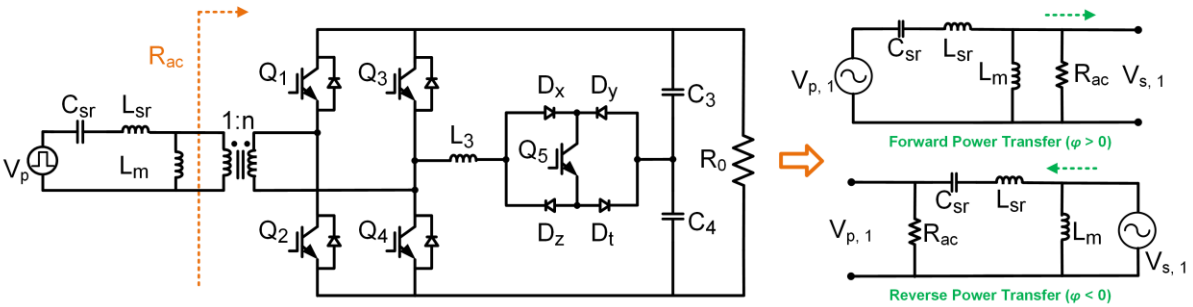

Figure 3.7. Equivalent circuit between the primary and secondary side of the proposed FPIBC

Simplified equivalent circuits with respect to the power flow direction between the primary and the secondary side of the proposed FPIBC are shown in Figure 3.7. Based on these simplified equivalent circuits, the steady-state characteristics of the bidirectional DC-DC converter with

series LC resonant tank can be derived from the fundamental harmonic approximation (FHA) (Mishima, Mizutani, and Nakaoka, 2017). $V_{p,1}$ and $V_{p,2}$ are the fundamental components of the square waves V_p and V_s as provided in Equation 10 and Equation 11.

$$V_{p1}(t) = \frac{4}{\pi} V_{bat} \sin w_s t \tag{10}$$

$$V_{s1}(t) = \frac{4}{\pi} K_f V_{bat} \sin\left(w_s t - \varphi\right) \tag{11}$$

The active power is delivered through the phase shift (φ) between V_p and V_s. The dc gains of the resonant converter when φ>0 (forward power transfer) and φ<0 (reverse power transfer) can be obtained as given in Equation 12 and Equation 13 respectively (Nasiri and Jean-Pierre, 2020).

$$\begin{aligned} K_f &= \frac{\left(\frac{sL_m R_{ac}}{sL_m + R_{ac}}\right)}{sL_{sr} + \left(\frac{1}{sC_{sr}}\right) + \left(\frac{sL_m R_{ac}}{sL_m + R_{ac}}\right)} \\ &= \frac{1}{\left(\frac{sL_{sr}}{R_{ac}}\right) + \left(\frac{L_{sr}}{L_m}\right) + \left(\frac{1}{sC_{sr}R_{ac}}\right) + \left(\frac{1}{s^2 L_m C_{sr}}\right) + 1} \end{aligned} \tag{12}$$

$$K_r = R_{ac} + \left(\frac{1}{sC_{sr}}\right) + sL_{sr} + sL_m \tag{13}$$

where L_m represents the magnetizing inductance of the transformer, and R_{ac} denotes the reflected load resistance value, which is calculated below:

$$R_{ac} = \frac{8n^2}{\pi^2} R_o \tag{14}$$

The equivalent output resistance of the resonant tank known as the reflected load resistance (R_{ac}) can be expressed as shown in Equation 14. Between the primary and secondary sides of the transformer is a turn ratio (n) that can be expressed in terms of the number of windings, voltage and current rates. Transformer turn ratio can be defined as *n*.

The load resistance R_o for both the forward and reverse power transfer modes can be formulated as in Equation 15 and Equation 16 respectively:

$$R_{0,f} = \frac{V_{dc}{}^2}{P_{dc}} = R_1 + R_2 \tag{15}$$

$$R_{0,r} = \frac{V_{bat}{}^2}{P_{bat}} \tag{16}$$

The DC gains of the resonant converter for Equation 12 and Equation 13 can be rearranged as follows:

$$K_f\left(Q,\ m,\ F_x\right) = \frac{1}{\sqrt{\left[1+\frac{1}{m}-\frac{1}{mF_x^2}\right]^2 + \left(F_x - \frac{1}{F_x}\right)^2 Q^2}} \tag{17}$$

$$K_r\left(Q,\ F_x\right) = \sqrt{1+\left(F_x - \frac{1}{F_x}\right)^2 Q^2} \tag{18}$$

In Equation 17 and Equation 18, *Q* is the quality factor, *m* is the ratio of total primary inductance to resonant inductance, and F_x is the normalized switching frequency. These parameters affect the DC voltage gain of the resonant converter. These parameters are described with the following equations (Equation 19 - 22):

$$Q = \frac{\sqrt{\frac{L_{sr}}{C_{sr}}}}{R_{ac}} \tag{19}$$

Equation 19 shows that Q is obtained by dividing the square root of the ratio of resonant inductance (L_{sr}) to resonant capacitance (C_{sr}) by reflected load resistance. Q value depends on the load current. As equation 18 shows, adjusting the Q value can significantly help achieve maximum voltage gain.

Ratio of the magnetizing inductance of the transformer (L_m) to the resonant inductance, m, is another crucial parameter that affects the voltage gain of the resonant tank as calculated below:

$$m = \frac{L_m}{L_{sr}} \tag{20}$$

The normalized switching frequency F_x is defined as the ratio of the switching frequency (f_s) to the resonant frequency (f_r) by the following formula (Equation 21). Accurate calculation of this parameter is also very important for achieving maximum DC gain.

$$F_x = \frac{f_s}{f_r} \tag{21}$$

"f_r" is the resonant frequency which is expressed below:

$$f_r = \frac{1}{2\pi\sqrt{L_{sr}C_{sr}}} \tag{22}$$

where L_{sr} denotes the resonant inductance in Henry, C_{sr} denotes the resonant capacitance in Farad and f_r denotes the resonant frequency in Hertz.

The power transfer between the primary and secondary sides is based on the direction of the phase shift angle (φ). The phase shift modulation method determines the operating principle of the bidirectional based DC-DC converter. Power circuit configuration of the bidirectional DC-DC converter is shown in Figure 3.8. If the phase shift angle is negative, a power transfer takes place from the secondary side to the primary side. If the phase shift angle is positive, a power transfer is made from the primary side to the secondary side.

The transferred power from the primary side to the secondary side of the proposed converter could be calculated from either side. The output active power can be defined as (Li and Bhat, 2010):

$$P_o = \frac{8K_f}{\pi^2 Q(F - 1/F)} \sin\varphi \tag{23}$$

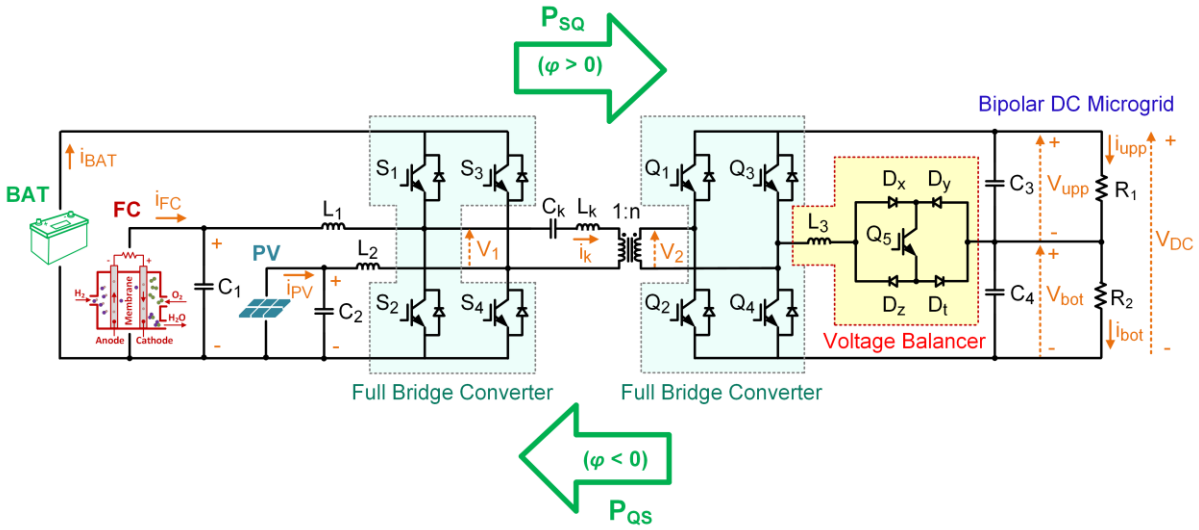

Figure 3.8. Power circuit configuration of the bidirectional DC-DC converter

The switching elements of power circuits are selected as IGBT because of the power rating and the switching frequency of the system. The total voltage in the bipolar DC microgrid V_{DC} is set to 200 V, and the upper and lower voltages are set to be divided equally (V_{upp} = V_{bot} = 100 V).

3.2. Operation Modes of Proposed Topology

The most common problems in MPCs such as power flow management and bipolar output voltage imbalances can easily be compensated by utilizing the proposed system which is composed of two full-bridge converters, a resonant tank and a voltage balancer circuit. As shown in Figure 3.9, the flowchart illustrates the general operating principle of the proposed system. "d_{bal}" represents the duty cycle of the balancing switch Q_5. According to the flowchart of the proposed system, initially the system parameters are defined and current/voltage measurements are performed, then the mode determination part is started. The mode

determination scheme is given in Figure 3.10 in detail. If the voltage imbalance occurs between the upper and lower output ports, the Q_5 switch is activated. Then, the enable signal to the switch comes in the form of 1/0 for balancing and a variable signal is generated. The controller detects any imbalance greater than 1 volt and activates the voltage balancer circuit. There is a hysteresis limit of 1 V in the voltage balancing operation. Phase shift modulation and proportional integral (PI) control techniques are used for this balancing process.

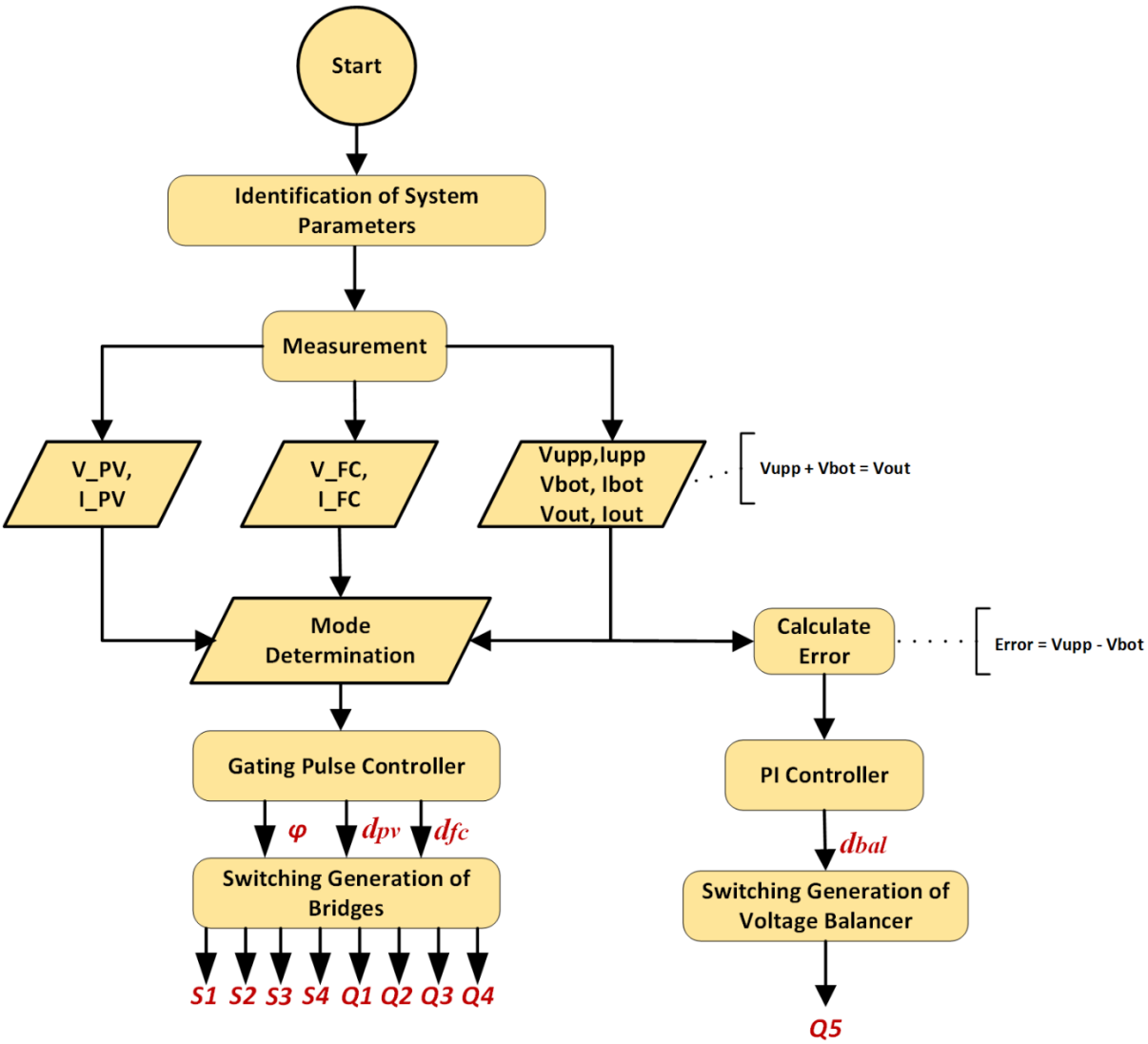

Figure 3.9. Flowchart of the overall system

The proposed converter operates at three different modes according to power flow scenarios and the power requirement of the load as illustrated in Figure 3.10. The operation mode is determined considering the available powers of PV, FC, and battery with the demand of the load. According to the mode determination flowchart, it is first checked whether the PV

produces power. If the PV power is not available, the proposed converter will operate in Mode 3 when the battery and the FC are able to meet the power demanded by the load. If the PV produces power, the converter will operate either in Mode 2 or in Mode 1.

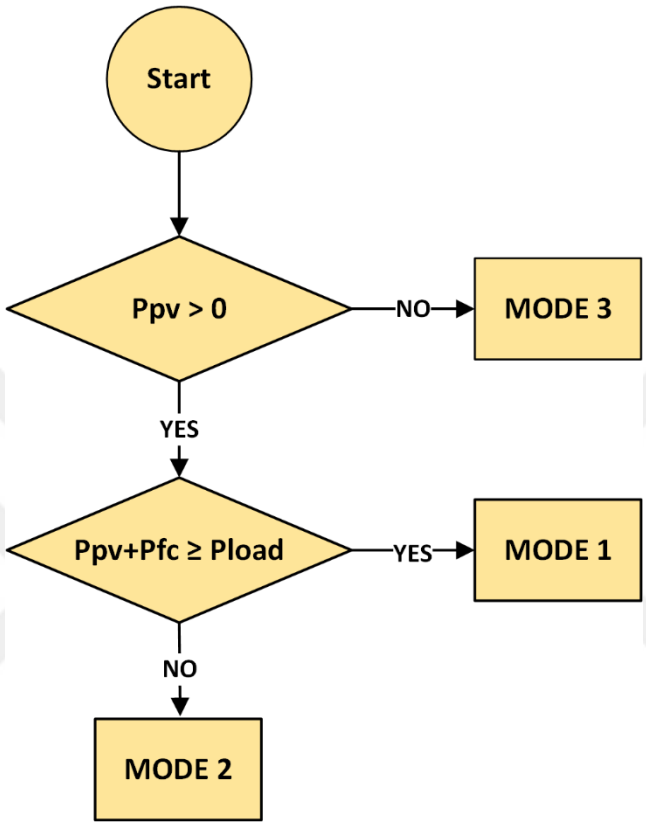

Figure 3.10. Flowchart for control logic of mode determination

Mode 1: Although there is solar radiation in this mode, the PV power is less than the power demanded by the load on the BPDCMG side and is not sufficient to supply the load alone. The load is fed by both PV and FC if the overall power of PV and FC is greater than the load demand. In this case, the battery is charged to absorb the surplus of renewable energy. When a power transfer scenario is defined as T for different operation modes of m_1, m_2, m_3, the following formula describes Mode 1 and the power flow between the ports.

$$\exists m_1 \in T: \ \left(P_{pv} > 0\right) \wedge \left(P_{pv} + P_{fc} \geq P_{load}\right)$$
$$P_{bat} = P_{pv} + P_{fc} - P_{load} \tag{24}$$

Mode 2: In this mode, the load demand is greater than the total amount of PV and FC power. The deficiency of power should be provided by the battery, which is discharged its previous charged power to support the RESs. Therefore, the load is fed by PV, FC and the battery. The operating condition of *Mode 2* and the power flow between the ports in this mode are given in the following equation.

$$\exists m_2 \in T:\ \left(P_{pv} > 0\right) \wedge \left(P_{pv} + P_{fc} < P_{load}\right) \\ P_{load} = P_{bat} + P_{pv} + P_{fc} \tag{25}$$

Mode 3: This mode corresponds to there is no solar power available and thus the load is fed by both FC and the battery. Since the FC power is not sufficient to supply the load alone, the battery is discharged by the proposed converter to assist the FC. The power flow between the ports is performed considering the following equation.

$$\exists\ m_3 \in T:\ \left(P_{pv} = 0\right) \\ P_{load} = P_{bat} + P_{fc} \tag{26}$$

To make the mode determination process more understandable, power flow scenarios given in Figure 3.11 can be examined.

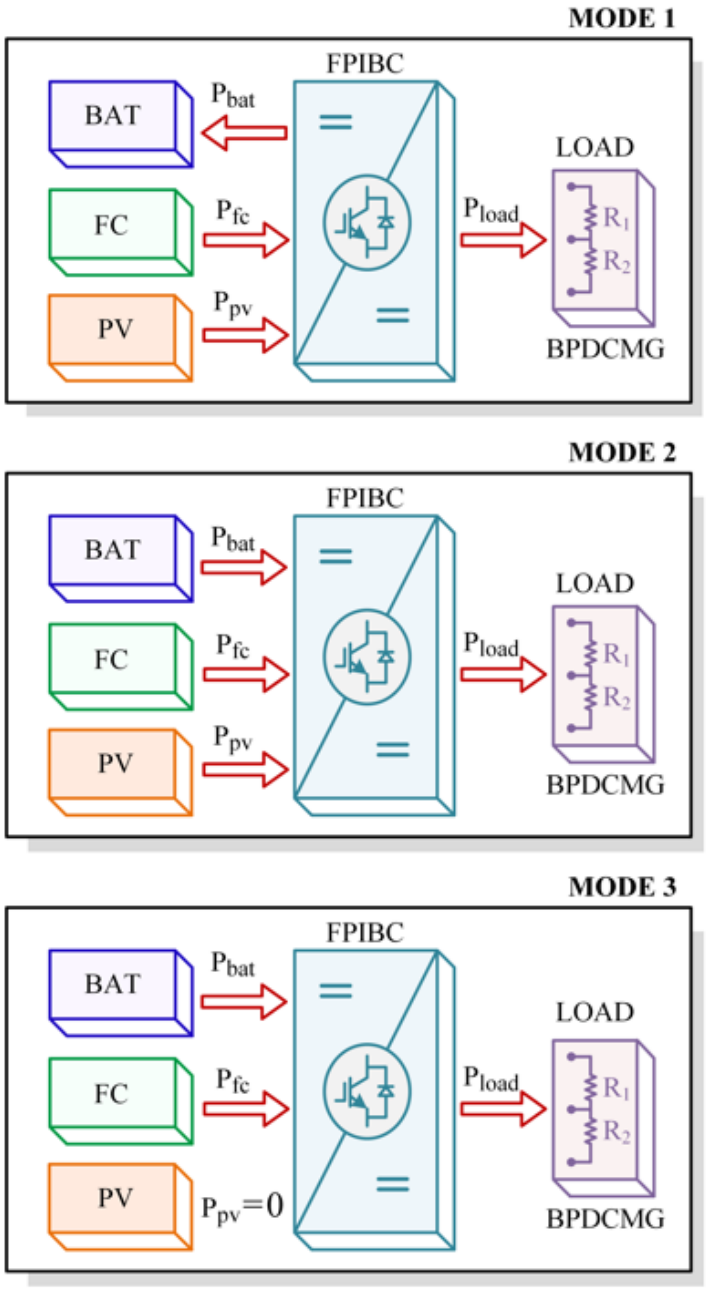

Figure 3.11. Power flow scenarios of the FPIBC

3.3. Control Scheme of FPIBC

The controller of the proposed system in this thesis is provided by four different control loops, as shown in Figure 3.12. These control loops are for the PV control loop, FC control loop, DC-link control loop and balancing control loop.

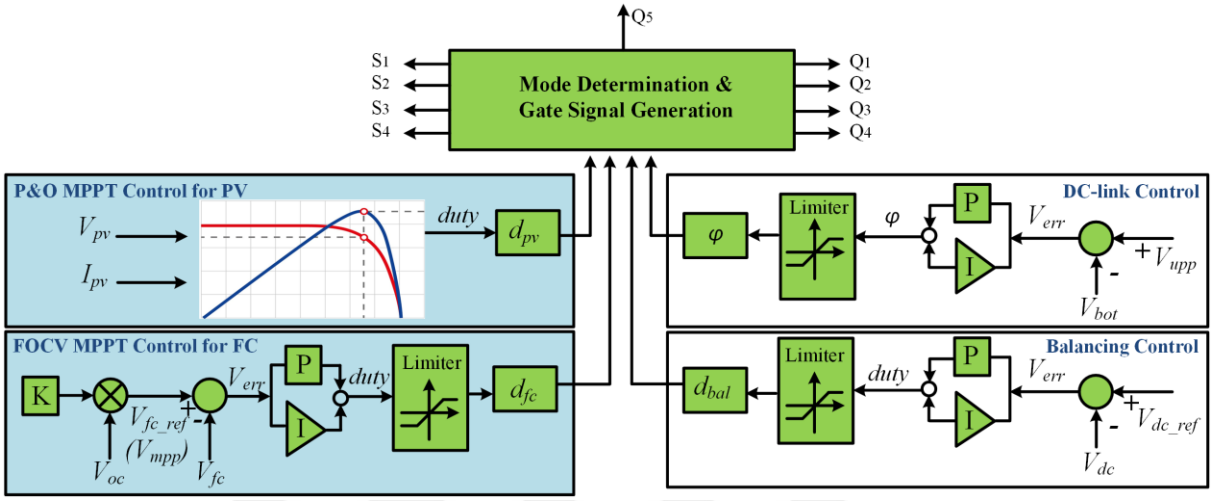

Figure 3.12. Multi-loop controller scheme of FPIBC

3.3.1. DC-Link Control

Single phase shift (SPS) modulation is the most widely used control method for bidirectional DC-DC converters, as it allows for high power transfer capabilities (Tan et al., 2012). The SPS modulation method is used in the controller of the DC-DC converter to enable bidirectional power flow and voltage control on both sides. Basic power transfer between primary and secondary sides is provided by the SPS modulation technique.

The phase shift modulation technique is applied in the DC-link control loop to keep the output voltage constant at 200 V (V_{dc_ref}). The error between the reference and measured output voltages is calculated in the related control loop. The phase-shift angle is generated by the controller after the error is transferred to the PI controller.

3.3.2. PV Control

In order to manage the power flow of the energy units, the PV and FC control loops adjust the duty cycle of the proposed converter's primary side switches. One of the voltage sources used in the structure presented is PV panels. The fluctuations in energy production in PV panels can occur due to the intermittent nature of renewable energy. In order to eliminate this problem,

various studies have been carried out in the literature. One of the most common methods used to ensure maximum power generation in PV panels is MPPT. The duty cycle of PV (d_{pv}) is computed using the PI controller considering the maximum operating point of the PV in the PV control loop. Perturb and observe (P&O) MPPT method is used to reach maximum operating point in PV system. Once the PV maximum operating voltage is determined, this value is selected as the reference value of the PI controller. Then, gate signals of the S_1 and S_2 switches are generated according to the duty cycle value and control of the PV system is completed. Maximum operating points of the PV array is given in Figure 3.13. In the given figure, the maximum operating voltage is 96 V, the maximum operating current is 38.5 A, and the optimum temperature is 25 °C at 1000 W/m^2.

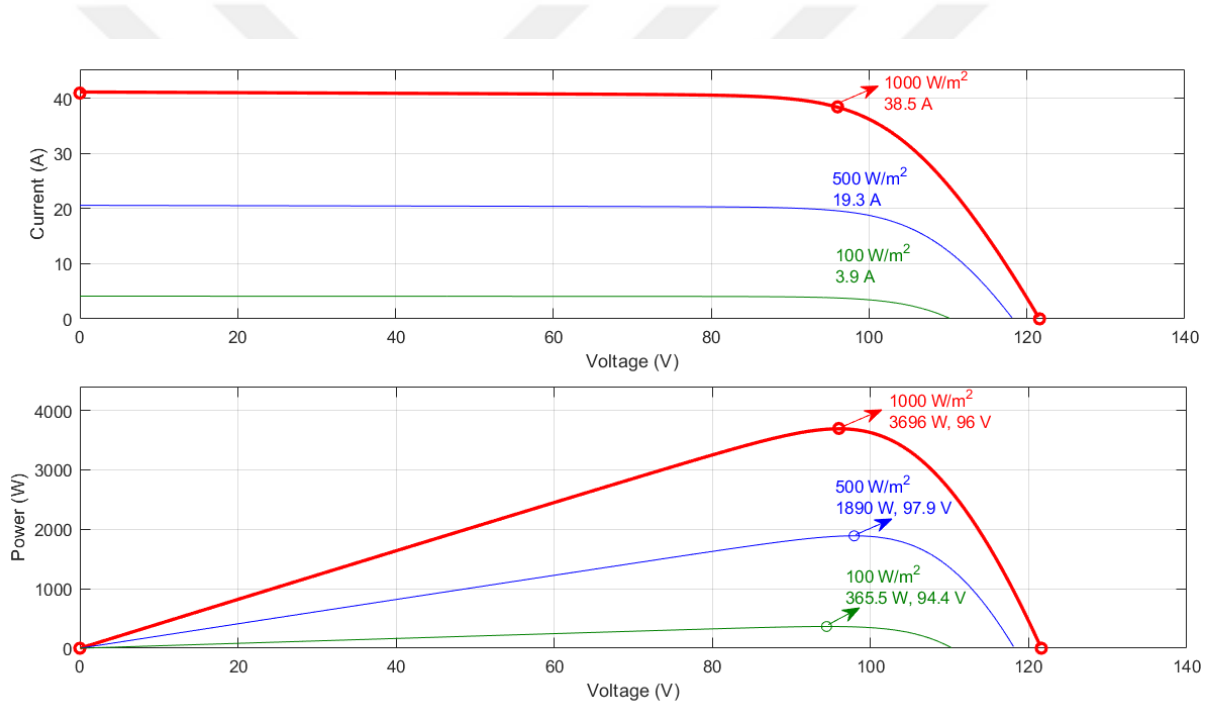

Figure 3.13. Maximum operating points of PV array at 25°C and specified irradiances

3.3.3. FC Control

The FC is one of the power sources in the proposed system. The FC control loop regulate the duty cycle of the presented converter's S_3 and S_4 switches. The duty cycle of FC (d_{fc}) is calculated using fractional open circuit voltage (FOCV) technique with PI controller considering the MPP of the FC in the FC control loop. The gate signals of the S_3 and S_4 switches are generated using this duty cycle value. The maximum operating voltage of FC (V_{mpp}) is obtained from Equation 27 (Luta & Raji, 2019). Where K is the voltage factor and V_{oc} is the

open circuit voltage of the FC stack. Typical values of K range from 0.7 to 0.8, and this parameter is 0.75 in the proposed controller.

$$V_{mpp} = KV_{oc} \tag{27}$$

3.3.4. Voltage Balancing Control

In bipolar DC microgrids, it is very important to provide compensation for voltage differences between upper and lower terminals. It has been observed in the literature survey that series-connected power converters or voltage balancers are used to achieve symmetrical bipolar output voltages. The aforementioned structures were examined in detail in the literature review section. In this thesis, a voltage balancer circuit topology consisting of four diodes and one active power switch was preferred. The control of the proposed voltage balancer structure is carried out by duty cycle adjustment of the Q_5 switch. The switching position of the Q_5 switch is critical in the operation of the voltage balancer circuit. V_{upp} and V_{bot} output voltages are monitored continuously to detect the imbalance condition in the BPDCMG. When the voltage difference of the output ports exceeds the hysteresis limit, the related controller regulates and enables the duty cycle of the Q_5 switch. The hysteresis limit for voltage balancing operation is 1 V and represented as α. The flowchart of the control algorithm of the voltage balancer is given in Figure 3.14.

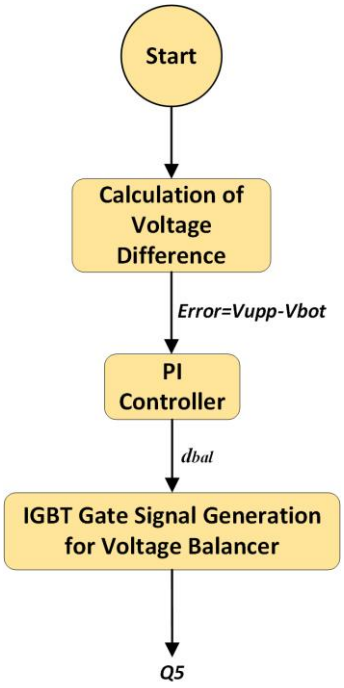

Figure 3.14. The flowchart of voltage balancer controller

The switching position of the Q_5 switch is determined by using Equation 28 and Equation 29 and considering the difference between V_{upp} and V_{bot} voltages. The controller initializes the balancing operation if the difference in voltage between upper side load voltage (V_{upp}) and bottom side load voltage (V_{bot}) is more than 1V.

$$Q5ON : (|Error| \geq \alpha) \tag{28}$$

$$Q5OFF : (|Error| < \alpha) \tag{29}$$

3.3.5. Gate Signal Generation

The outputs of the controller are the gate signals of the full-bridge converters. The PWM technique is used to generate the switching signals of the IGBTs. The primary bridge is composed of S_1, S_2, S_3 and S_4 while the secondary bridge is composed of Q_1, Q_2, Q_3 and Q_4 gate signals. The switching frequency of the full-bridge converters is selected as 20 kHz. All possible switching states and positions for one switching cycle of the proposed FPIBC is summarized in Table 3.1.

Table 3.1. Switching states and positions for one switching cycle

Switching States	Operating Conditions		Switching Conditions		
	Mode	Imbalance	S_1, S_2, S_3, S_4	Q_1, Q_2, Q_3, Q_4	Q_5
1	1, 2	No	0110	0110	0
2	1, 2	No	1010	1001	0
3	1, 2	No	1010	0110	0
4	1, 2	No	1001	0110	0
5	1, 2	No	1001	1001	0
6	1, 2, 3	Yes	0110	1001	1/0
7	1, 2, 3	Yes	0110	0110	1/0
8	1, 2, 3	Yes	1010	1001	1/0
9	1, 2, 3	Yes	1010	0110	1/0
10	1, 2, 3	Yes	1001	0110	1/0
11	1, 2, 3	Yes	1001	1001	1/0

The operating conditions and switching positions of the Q_5 switch, which controls the voltage balancer circuit, can also be seen in detail in this table. The relevant switches operate in two ways according to the presence of voltage imbalance status. If there is an imbalance, the gate signal of the Q_5 switch comes in the form of 1/0. If there is no imbalance, this switch is off and the gate signal is 0 continuously. As can be seen from the table, there are a total of eleven switching states. When the switching states in the table are examined, it is seen that there is no imbalance in the first five states and there is an imbalance in the other six states.

4. SIMULATION RESULTS AND DISCUSSIONS

4.1. MATLAB/Simulink Model of FPIBC and System Parameters

In order to verify the performance of the proposed multiport DC-DC converter topology and designed controllers, simulation results captured from MATLAB-Simulink software are presented. The effectiveness of the proposed FPIBC system is tested with different case studies. The overall MATLAB/Simulink model of the proposed FPIBC system is shown in Figure 4.1. The power circuit design parameters and control parameters of the proposed FPIBC used in simulation model are given in Table 4.1 - Table 4.4. Control algorithms of the DC-DC converter and voltage balancer circuit which are specified in Chapter 3, are formed with MATLAB code by using MATLAB editor. In this simulation study, it is aimed to provide the following features by exploring the different case studies:

- To observe the steady-state and dynamic response of the system under changing load conditions
- To monitor power flows between input and output ports in different operating modes depending on the change in RES and ESU parameters
- To demonstrate that the voltage imbalance between the lower and upper terminals of the bipolar DC microgrid can be successfully compensated

Table 4.1. MATLAB/Simulink Simulation Parameters

MATLAB/Simulink Parameters	
Solver Maximum Step Size	5e-07 s
Duration of Simulation Time	8 s

Table 4.2. Control System Parameters

DC-Link PI Control Parameters	
Kp	1.1
Ki	0.025

Table 4.3. Resonant Tank Design Parameters

Resonant Tank Parameters	
Forward DC Gain	0.89
Reverse DC Gain	1.1

Table 4.4. System Parameters of FPIBC Simulation Model

System	**Parameter**	**Value**
PV	PV maximum power (1000 W/m^2)	3696 W
	Maximum power point voltage (1000 W/m^2)	96 V
	Maximum power point current (1000 W/m^2)	38.5 A
	PV maximum power (500 W/m^2)	1890 W
	Maximum power point voltage (500 W/m^2)	97.9 V
	Maximum power point current (500 W/m^2)	19.3 A
	PV maximum power (100 W/m^2)	365.5 W
	Maximum power point voltage (100 W/m^2)	94.4 V
	Maximum power point current (100 W/m^2)	3.9 A
	PV capacitor (C_2)	1 mF
Battery	Capacity	5.4 Ah
	Nominal voltage	140 V
FC (SOFC)	Nominal power rating	4245 W
	Nominal operating point (I_n, V_n)	39.86 A, 106.5 V
	Open circuit voltage (V_{oc})	141.34 V
	Maximum power rating	4500 W
	Maximum operating point (I_m, V_m)	42.91 A, 104.86 V
	Number of cells	119
	Types of cells	Solid Oxide FC
	System temperature	873 K
	Nominal pressure	1.35 bar
	FC capacitor (C_1)	1 mF
Resonant Converter	Resonant inductance (L_{sr})	20 uH
	Resonant capacitance (C_{sr})	50 uF
	Resonant frequency (f_r)	~ 5 kHz
	Switching frequency (f_s)	20 kHz
	Transformer turns ratio (n)	1:1
DC Microgrid	Total load voltage (V_{DC})	200 V
	Upper side load voltage (V_{upp})	100 V
	Bottom side load voltage (V_{bot})	100 V
Other Circuit Parameters	$C_3 = C_4$	10 mF
	$L_1 = L_2$	2 mH
	L_3	18 uH

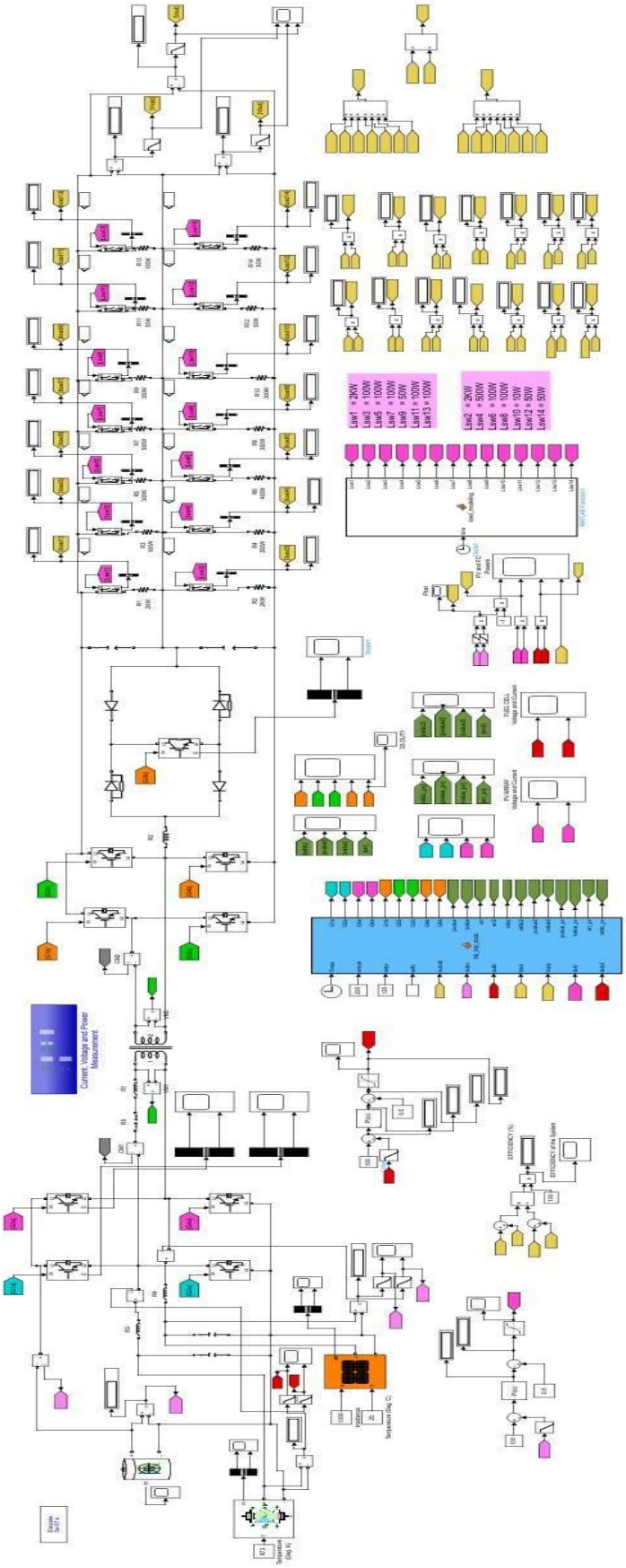

Figure 4.1. The simulation model of the proposed system

This section presents the proposed system's simulation model as well as simulation results obtained from different case studies. In order to evaluate the effectiveness and applicability of the proposed converter, three case studies are performed that are summarized in Table 4.5.

Table 4.5. Summary of Case Studies

	Time Interval	Fuel Cell Parameters	PV System Parameters	Unbalanced Load Condition	Load Power (P_{upp}, P_{bot})	Operation Mode
Case Study #1	t = 2-4 s	T = 873 K P = 0.6 bar	T = 25 °C Irr = 500 W/m^2	No	P_{upp} = 2100 W P_{bot} = 2100 W	Mode 1
	t = 4-5 s	T = 873 K P = 0.6 bar	T = 25 °C Irr = 500 W/m^2	No	P_{upp} = 2700 W P_{bot} = 2700 W	Mode 2
	t = 5-6 s	T = 873 K P = 0.14 bar	T = 25 °C Irr = 500 W/m^2	No	P_{upp} = 2700 W P_{bot} = 2700 W	Mode 2
	t = 6-7 s	T = 873 K P = 0.14 bar	T = 25 °C Irr = 500 W/m^2	No	P_{upp} = 2400 W P_{bot} = 2400 W	Mode 2
	t = 7-8 s	T = 873 K P = 0.21 bar	T = 25 °C Irr = 500 W/m^2	No	P_{upp} = 2400 W P_{bot} = 2400 W	Mode 2
Case Study #2	t = 2-3 s	T = 873 K P = 1.35 bar	T = 25 °C Irr = 500 W/m^2	No	P_{upp} = 2200 W P_{bot} = 2200 W	Mode 1
	t = 3-5 s	T = 873 K P = 1.35 bar	T = 25 °C Irr = 500 W/m^2	Yes	P_{upp} = 3400 W P_{bot} = 2900 W	Mode 2
	t = 5-6 s	T = 873 K P = 1.35 bar	T = 25 °C Irr = 1000 W/m^2	No	P_{upp} = 3000 W P_{bot} = 3000 W	Mode 1
	t = 6-8 s	T = 873 K P = 1.35 bar	T = 25 °C Irr = 1000 W/m^2	Yes	P_{upp} = 2400 W P_{bot} = 2500 W	Mode 1
Case Study #3	t = 2-4 s	T = 873 K P = 0.7 bar	T = 25 °C Irr = 1000 W/m^2	Yes	P_{upp} = 2300 W P_{bot} = 2650 W	Mode 1
	t = 4-5 s	T = 873 K P = 0.7 bar	T = 25 °C Irr = 1000 W/m^2	Yes	P_{upp} = 3000 W P_{bot} = 2900 W	Mode 1
	t = 5-8 s	T = 873 K P = 0.7 bar	T = 25 °C Irr = 0 W/m^2	Yes	P_{upp} = 3250 W P_{bot} = 3000 W	Mode 3

4.2. Case Study 1

The first case study highlights the performance of mode 1, mode 2 and transition performance between the related modes, as well as, the effect of changes in FC pressure on the system. The performance of the proposed system is investigated by changing FC pressure and balanced load conditions. The parameters of the Case Study 1 are summarized in Table 4.6. The solar irradiation value was kept constant at 500 W/m^2 during this case. Total simulation time is divided into five intervals according to the load power (P_{load}) variations and FC pressure variations. In this case, there is no imbalance between upper and lower loads.

The battery voltage and current are demonstrated in Figure 4.2 and Figure 4.3 respectively. Figure 4.4 shows the SOC of the battery. The DC link voltage of the BPDCMG side is depicted in Figure 4.5. The PV power, the FC power and the battery power are shown in Figure 4.6, Figure 4.7, and Figure 4.8 respectively. In the time interval of 2-4 s, total power demanded by the load is 4200 W as seen from Figure 4.9. The powers of the upper and lower loads are equal and 2100 W. Demanded power of load for Case Study 1 is given in Figure 4.9. FC pressure was kept constant at 0.6 bar from t=2 to t=5. FC and PV meet the power demanded by the load where FC power is approximately 3386.39 W and PV power is about 1889.68 W. The battery is charging from t=2 s to t=4 s. The SOC of the battery is changing from 50.05% to 49.9%. The battery absorbs the surplus power of 765.1 W. As understood from the Figure 4.10, the system operates in mode 1 and the peak efficiency of the system is 93.27 % in this time interval.

As seen in the Figure 4.9, the power demanded by the load increases to 5400 W at t=4 s. The powers of the upper and lower loads are equal and 2700 W and there is no imbalance condition. At t=4 s, the battery initiates to discharge and the system operating mode switches from mode 1 to mode 2 (see in Figure 4.4). As given in the Figure 4.2 and Figure 4.3, at t=4 s, the battery voltage decreases to 150.013 V from 151.782 V, and the battery current increases to 2.252 A from -5.042 A. After t=4 s, the primary side energy units including battery, PV and FC supply the demanded load power.

Then, at t=5 s, the FC pressure value reduces to 0.14 bar from 0.6 bar. At t=5 s, FC power decreases to 2617.34 W from 3468.91 W (see in Figure 4.8), and the battery power increases to 1165.5 W from 341.6 W (see in Figure 4.7). PV power for Case Study 1 is given in Figure 4.6. It is observed that the power supplied by FC (P_{fc}) is decreased depending on pressure

change in the time interval of 5-6 s. FC power for Case Study 1 is illustrated in Figure 4.8. At t=6 s, the power demanded by the load reduces to 4800 W. It is detected that the FC pressure value increases to 0.21 bar from 0.14 bar while passing to the last time interval of 7-8 s, consequently, the FC power increases slightly.

In short, as a result of this case study, it is seen that system efficiency is preserved and V_{DC} remains constant even if the power values at the input ports and the total load power change (see in Figure 4.5). Moreover, it is concluded that the FC pressure changes affect the P_{fc}.

Table 4.6. Summary of Case Study 1

Time Interval	Fuel Cell Parameters	PV System Parameters	Unbalanced Load Condition	Load Power (P_{upp}, P_{bot})	Operation Mode
t = 2-4 s	T = 873 K P = 0.6 bar	T = 25 ºC Irr = 500 W/m^2	No	P_{upp} = 2100 W P_{bot} = 2100 W	Mode 1
t = 4-5 s	T = 873 K P = 0.6 bar	T = 25 ºC Irr = 500 W/m^2	No	P_{upp} = 2700 W P_{bot} = 2700 W	Mode 2
t = 5-6 s	T = 873 K P = 0.14 bar	T = 25 ºC Irr = 500 W/m^2	No	P_{upp} = 2700 W P_{bot} = 2700 W	Mode 2
t = 6-7 s	T = 873 K P = 0.14 bar	T = 25 ºC Irr = 500 W/m^2	No	P_{upp} = 2400 W P_{bot} = 2400 W	Mode 2
t = 7-8 s	T = 873 K P = 0.21 bar	T = 25 ºC Irr = 500 W/m^2	No	P_{upp} = 2400 W P_{bot} = 2400 W	Mode 2

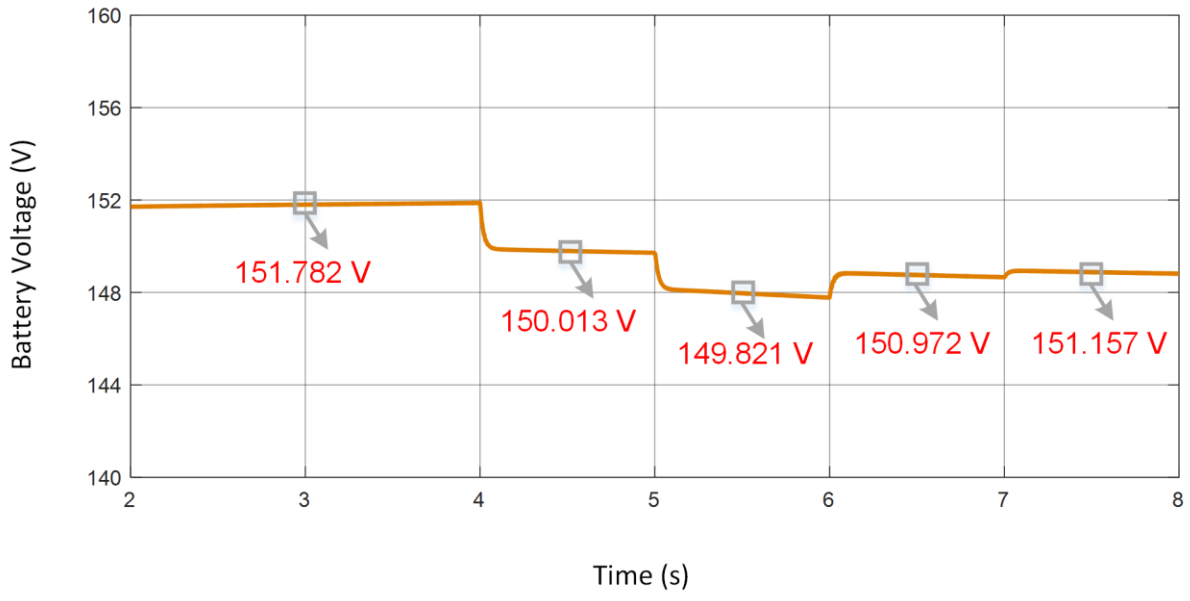

Figure 4.2. The battery voltage for Case Study 1

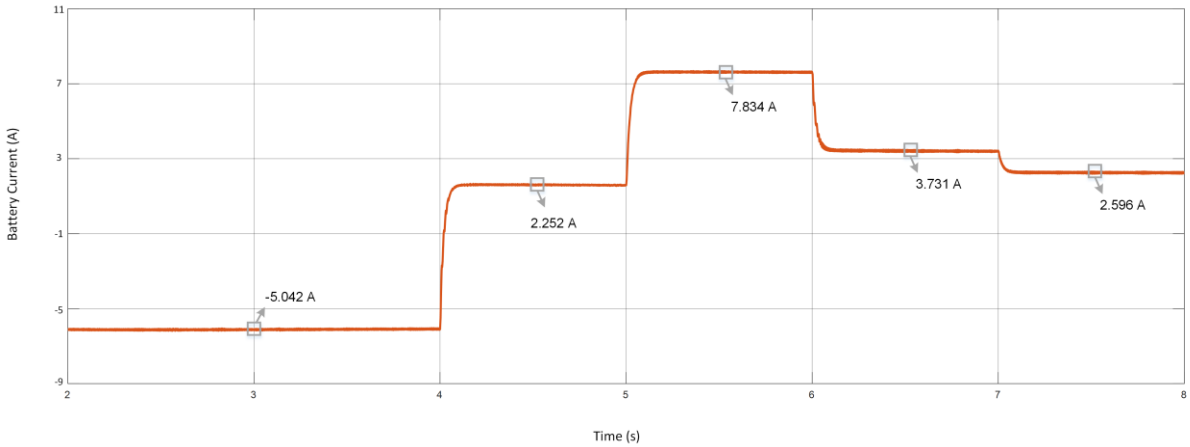

Figure 4.3. The battery current for Case Study 1

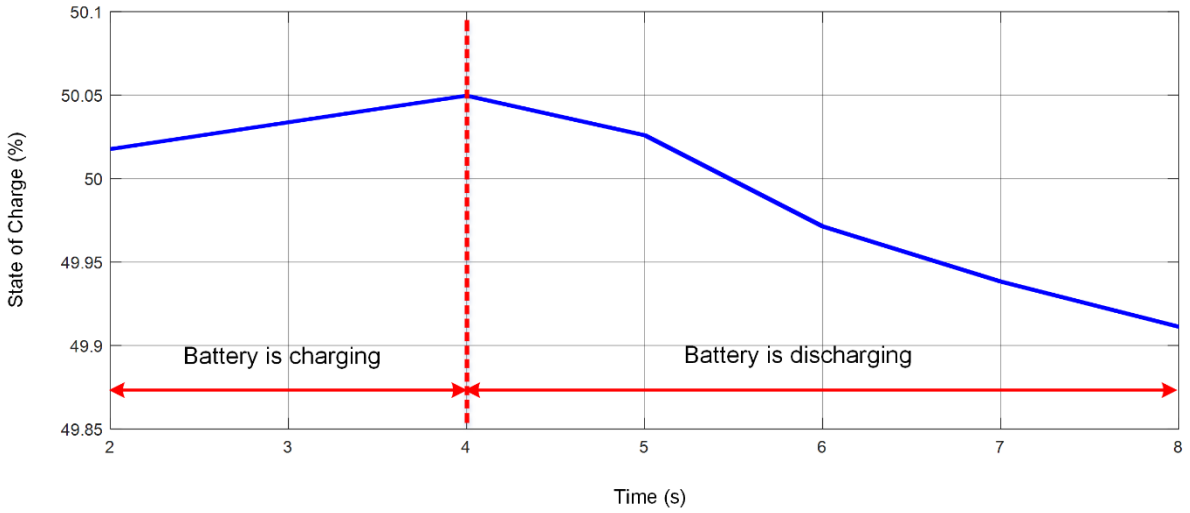

Figure 4.4. The SOC of the battery for Case Study 1

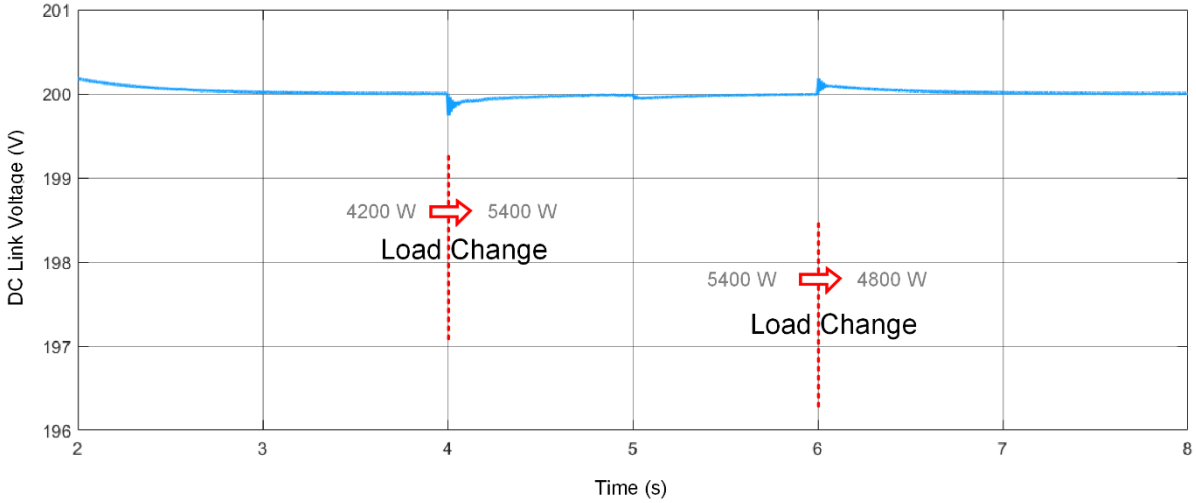

Figure 4.5. DC link voltage for Case Study 1

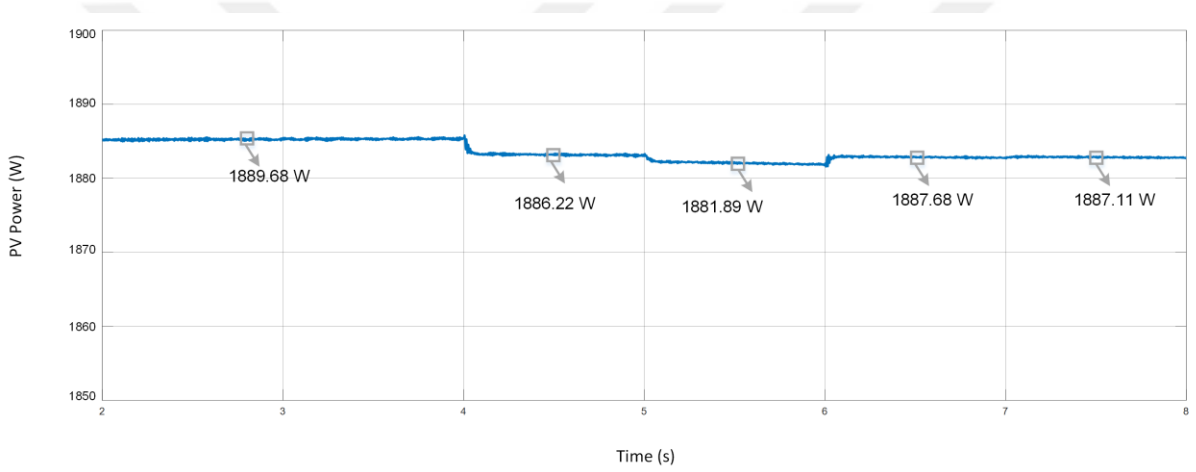

Figure 4.6. PV power for Case Study 1

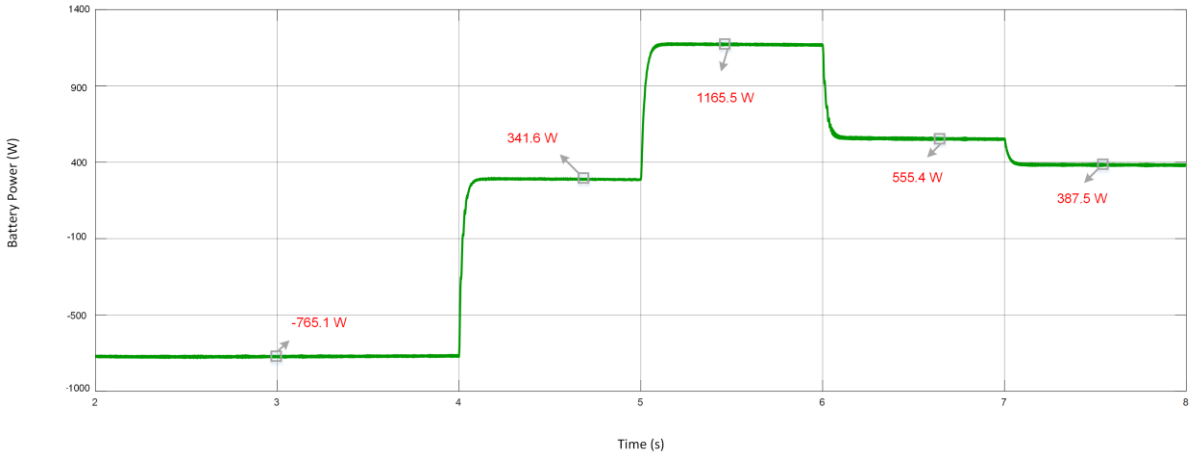

Figure 4.7. Battery power for Case Study 1

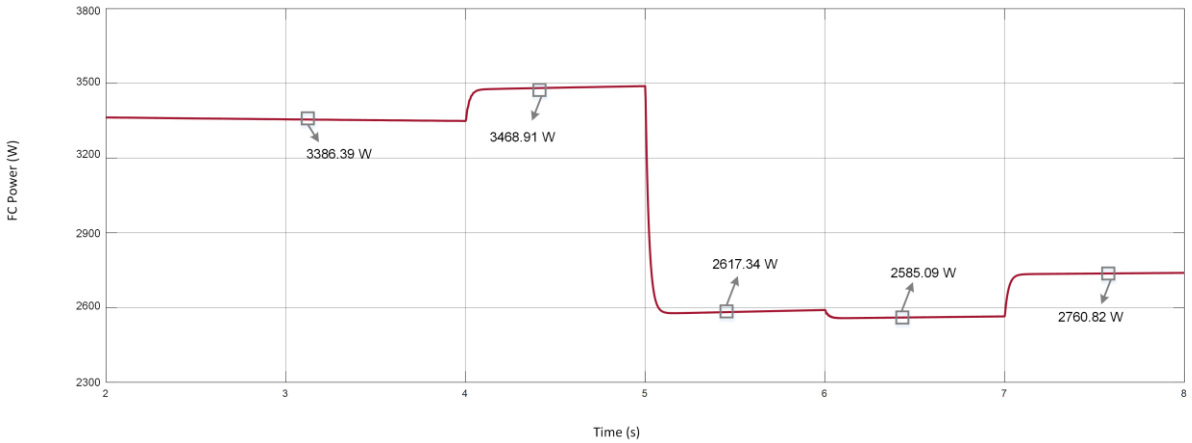

Figure 4.8. FC power for Case Study 1

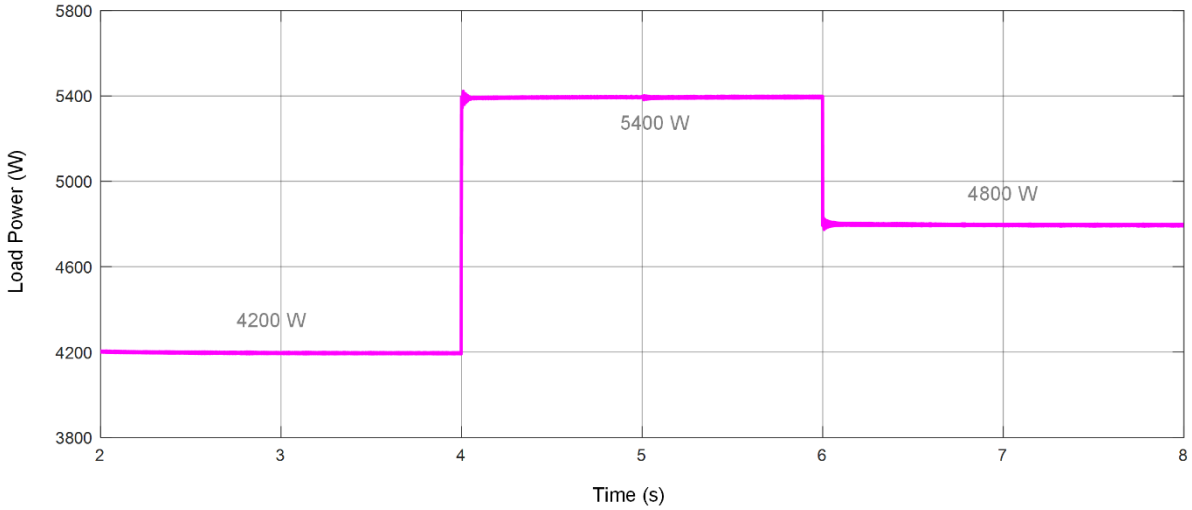

Figure 4.9. Demanded power of load for Case Study 1

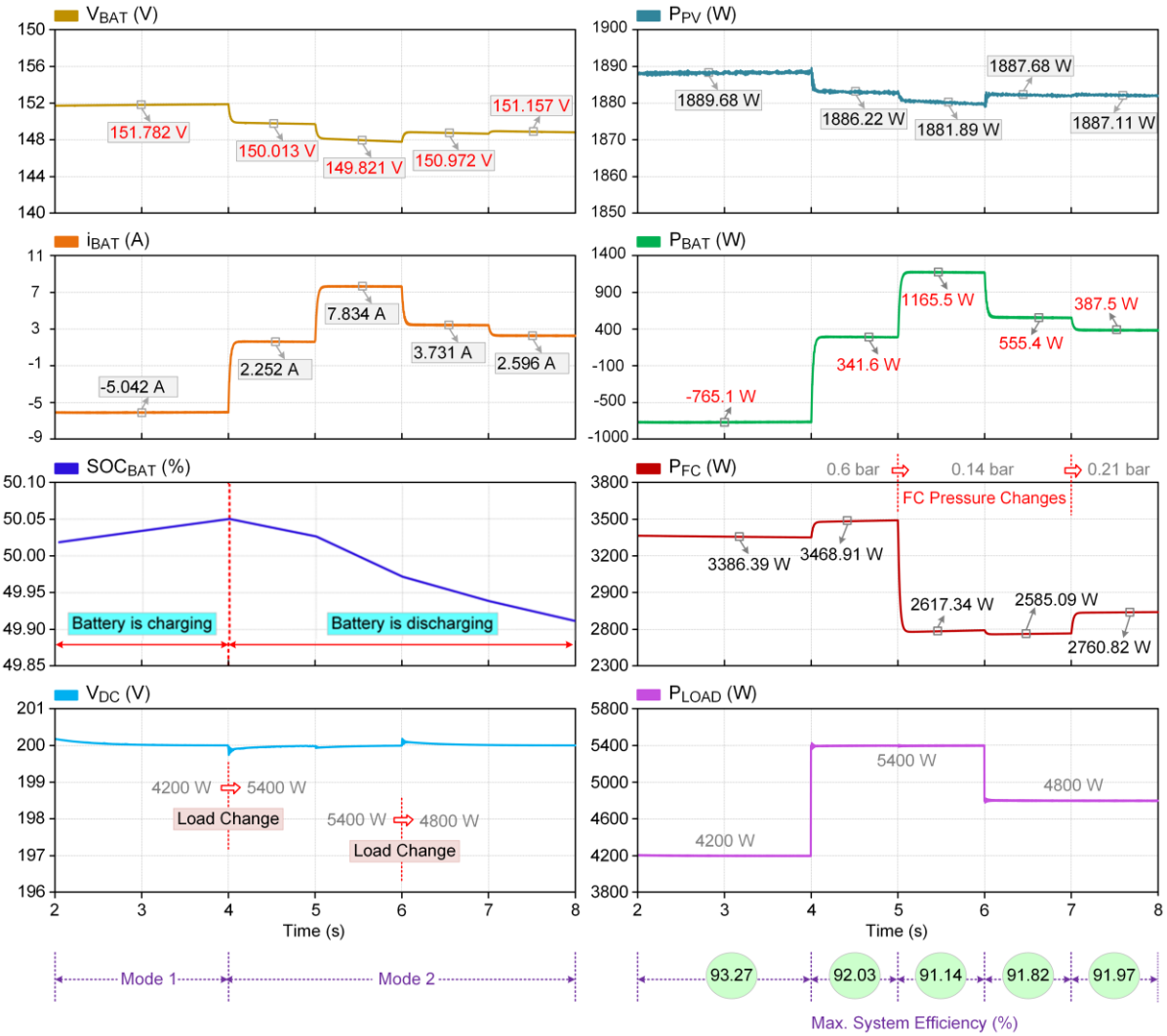

Figure 4.10. Summary of simulation results for Case Study 1

4.3. Case Study 2

In the second case study, it is aimed to show the performance of the voltage balancer circuit. The second case study also presents the performance of the proposed converter during mode 1, mode 2, and load transition. The transition moments from both mode 1 to mode 2 and from mode 2 to mode 1 are examined, unlike the first case study. Moreover, the effect of change in PV solar irradiation on the proposed system is investigated. The FC pressure value was kept constant at 1.35 bar throughout this case study. The parameters of the Case Study 2 are listed in Table 4.7. In this case study, there are a total of four time intervals according to the load power changes and solar irradiation variations. In each interval, there was an imbalance between the P_{upp} and P_{bot} powers, while the total load power was changed in each interval.

The PV voltage and current are demonstrated in Figure 4.11 and Figure 4.12 respectively. Figure 4.13 shows the SOC of the battery. The DC link voltage of the BPDCMG side is depicted in Figure 4.14. The PV power, the FC power and the battery power are shown in Figure 4.15, Figure 4.16, and Figure 4.17 respectively. In the time interval of 2-3 s, the total power demanded by the load is 4400 W. The powers of the upper and lower loads are equal and 2200 W. Demanded power of load for Case Study 2 is given in Figure 4.18. The solar irradiation was kept constant at 500 W/m^2 from t=2 to t=5. The battery is charging from t=2 s to t=3 s. FC and PV produce the power demanded by the load, while the battery is charged. FC power for Case Study 2 is demonstrated in Figure 4.17. As seen in Figure 4.19, the system operates in mode 1 and the peak efficiency of the system is 93.56 % in this time interval.

As shown in Figure 4.19, the power demanded by the load increases to 6300 W at t=3 s. The time interval of 3-5 s represents mode 2 with 500 W/m^2 irradiation, 25 ^{o}C, and 6300 W demand. In the time interval of 3-5 s, a 500 W imbalance occurred between the power of the upper and lower loads. At t=3 s, the system operating mode is switched from mode 1 to mode 2. As seen in the Figure 4.13, from t=3 s to t=5 s, the battery is operated in discharging mode.

At t=5 s, while the solar irradiation value increases to 1000 W/m^2 from 500 W/m^2, the Pload value reduces to 6000 W from 6300 W. The solar irradiation was kept constant at 1000 W/m^2 from t=5 to t=8. At t=5 s, PV current increases to 39.51 A from 20.04 A (see in Figure 4.12), and PV power increases to 3689.3 W from 1868.8 W. Moreover, as shown in Figure 4.16, the battery power decreases to -1479.82 W from 502.24 W at t=5 s. It is observed that the power

supplied by PV (P_{pv}) is increased depending on solar irradiation change in the time interval of 5-6 s. PV power for Case Study 2 is illustrated in Figure 4.15. There is no imbalance between upper and lower loads in the 5-6 s interval. It is concluded that the condition of the battery power flow is altered from charging to discharging with the transition from mode 2 to mode 1 at the t=5 s. Afterward, an imbalance occurred again at t=6 s. The magnitude of this imbalance was 100 W and the total demanded power (P_{load}) was 4900 W. The system operates in mode 1 and the battery is operated in charging mode in this time interval (5-8 s). Mode transitions and all the changes mentioned above are detailed in Figure 4.19.

Briefly, when the solar irradiation value is changed and imbalances occur between loads, it is concluded that DC microgrid voltage values remain constant (see in Figure 4.14) and equal thanks to the proposed controller and voltage balancer circuit. As seen in Figure 4.19, the maximum efficiency value of the system is 94.85% in P_{load} = 4900 W in this case. PV current-voltage, the SOC of the battery, DC microgrid voltage values, and all port's power values were demonstrated in Figure 4.11 - 4.18 for Case Study 2.

Additionally, in order to validate the effectuality of the voltage balancer circuit, Figure 4.29 is presented. Thus, the ability to compensate for voltage differences on the upper and lower load sides of the DC microgrid with and without balancing is signified. It was observed that voltage differences are compensated by the voltage balancer circuit as shown in Figure 4.29.

Table 4.7. Summary of Case Study 2

Time Interval	Fuel Cell Parameters	PV System Parameters	Unbalanced Load Condition	Load Power (P_{upp}, P_{bot})	Operation Mode
t = 2-3 s	T = 873 K P = 1.35 bar	T = 25 °C Irr = 500 W/m^2	No	P_{upp} = 2200 W P_{bot} = 2200 W	Mode 1
t = 3-5 s	T = 873 K P = 1.35 bar	T = 25 °C Irr = 500 W/m^2	Yes	P_{upp} = 3400 W P_{bot} = 2900 W	Mode 2
t = 5-6 s	T = 873 K P = 1.35 bar	T = 25 °C Irr = 1000 W/m^2	No	P_{upp} = 3000 W P_{bot} = 3000 W	Mode 1
t = 6-8 s	T = 873 K P = 1.35 bar	T = 25 °C Irr = 1000 W/m^2	Yes	P_{upp} = 2400 W P_{bot} = 2500 W	Mode 1

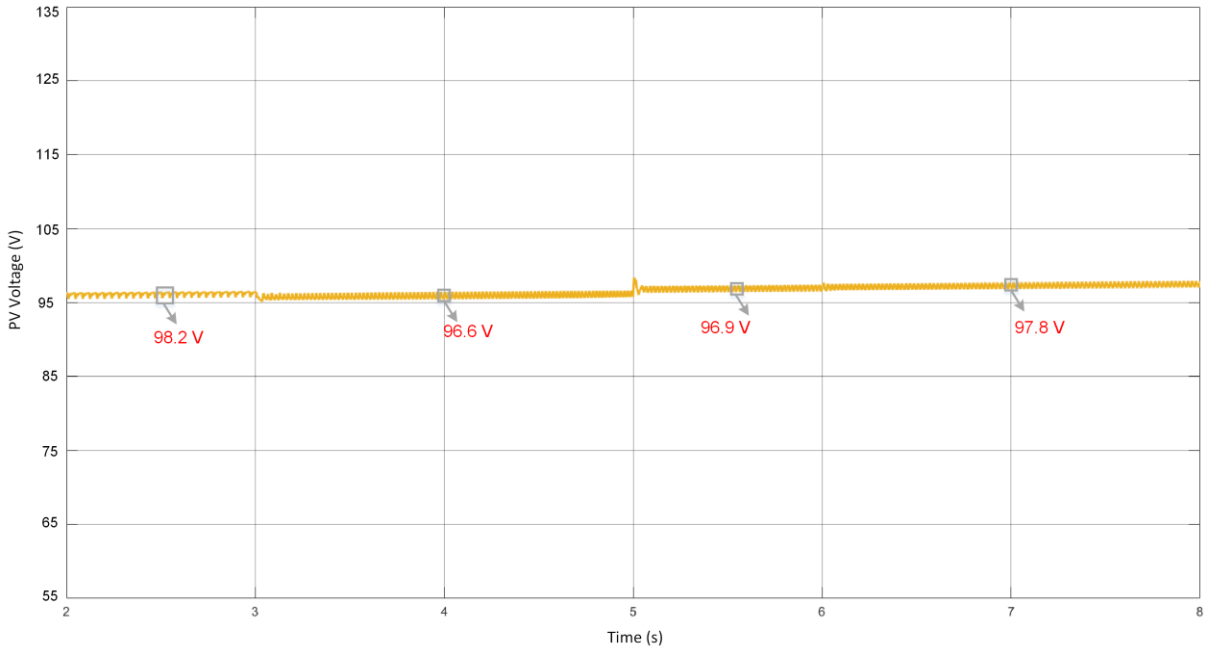

Figure 4.11. The PV voltage for Case Study 2

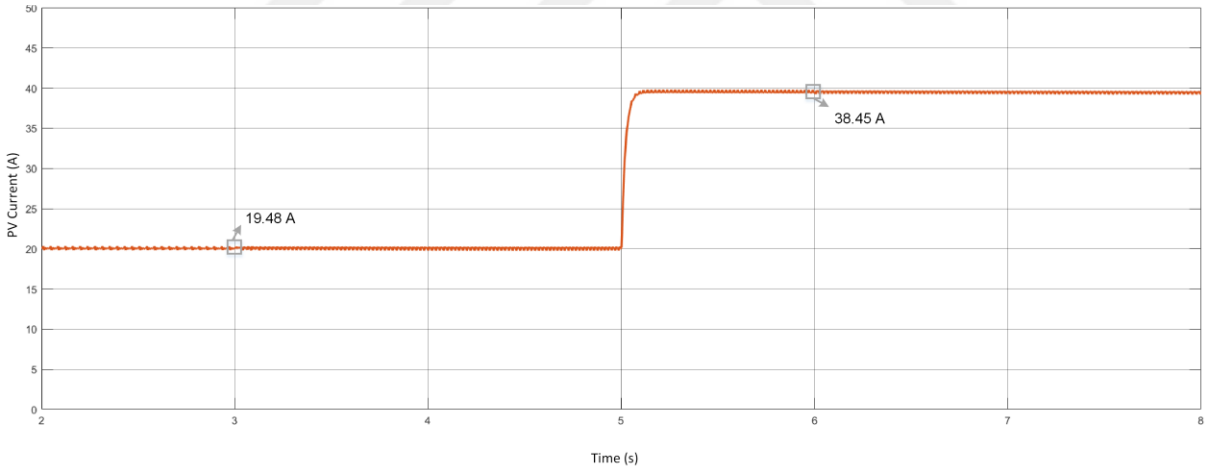

Figure 4.12. The PV current for Case Study 2

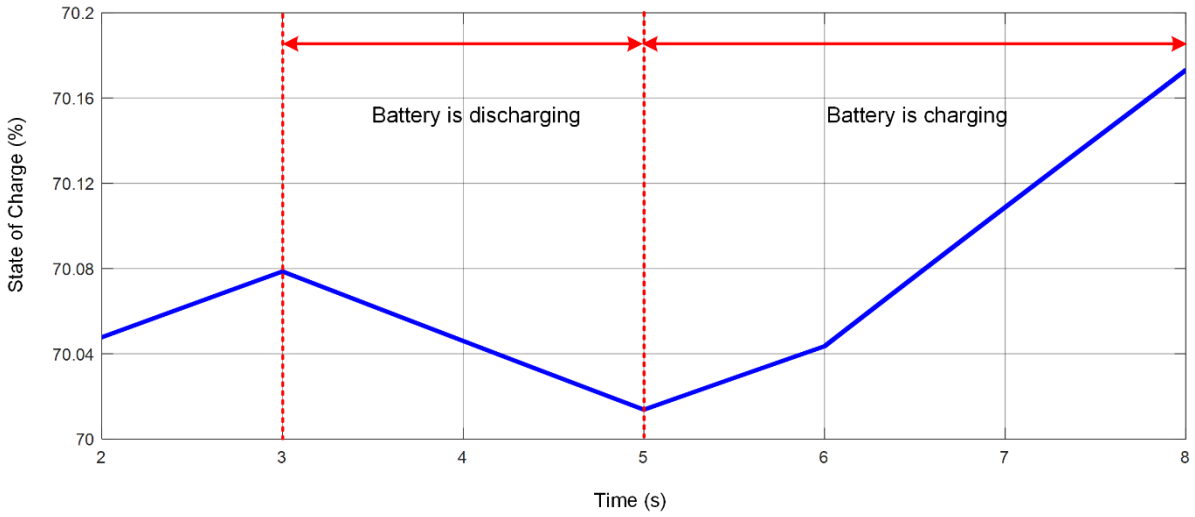

Figure 4.13. The SOC of the battery for Case Study 2

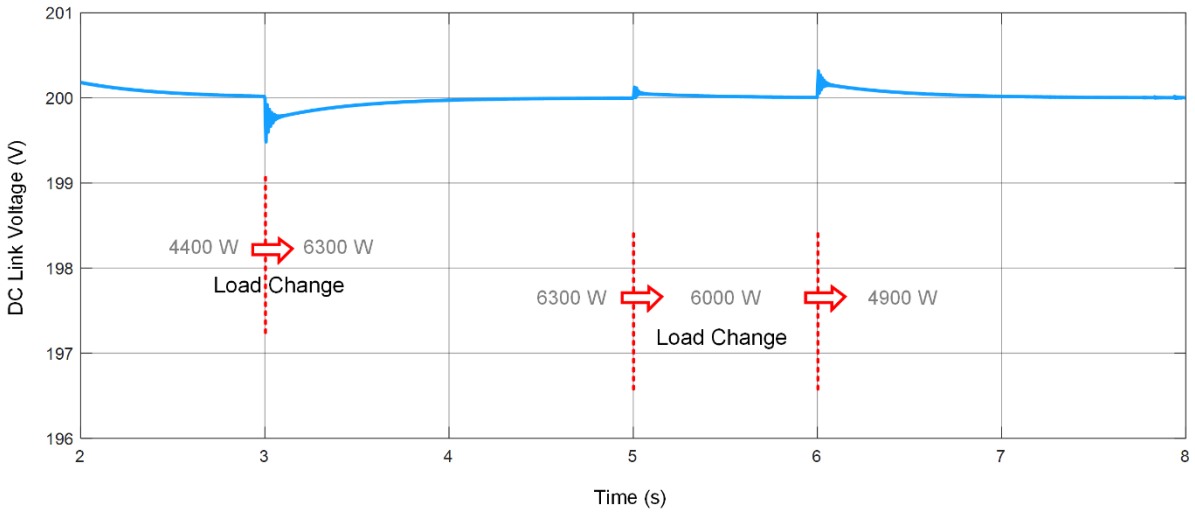

Figure 4.14. DC link voltage for Case Study 2

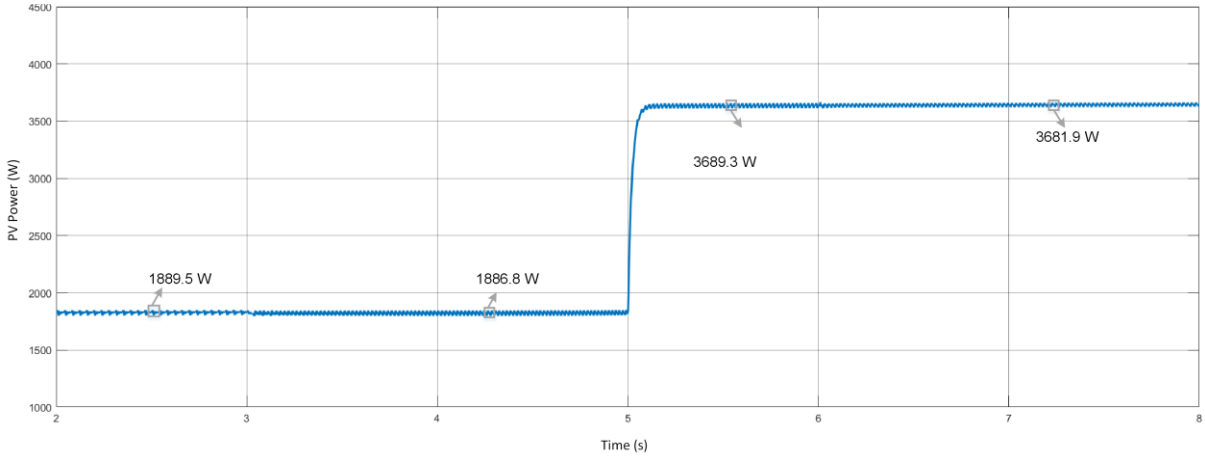

Figure 4.15. PV power for Case Study 2

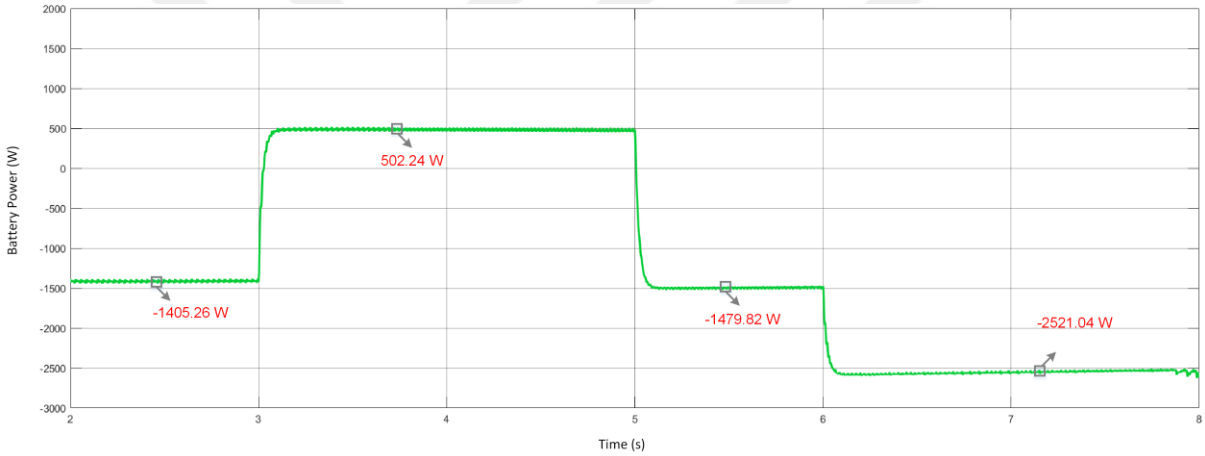

Figure 4.16. Battery power for Case Study 2

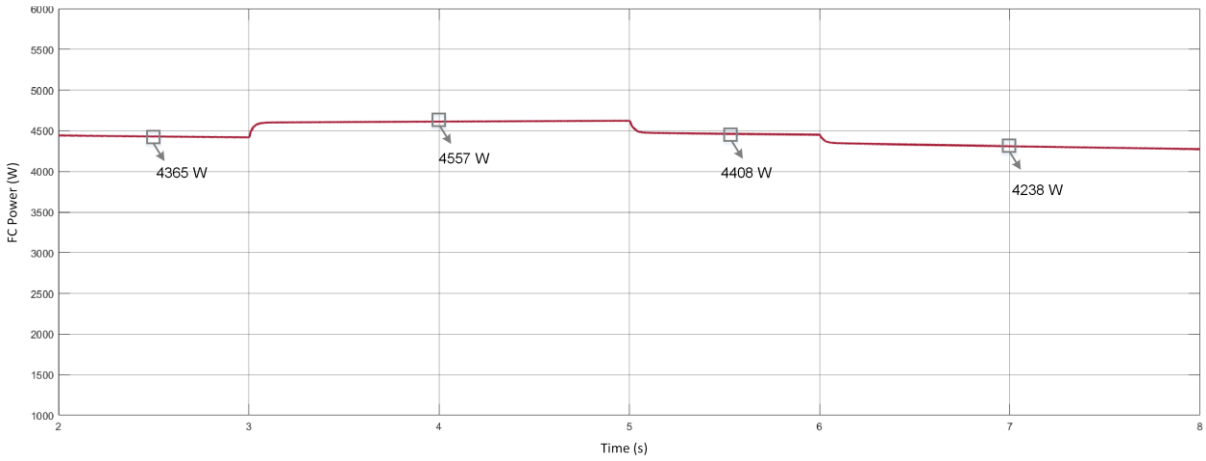

Figure 4.17. FC power for Case Study 2

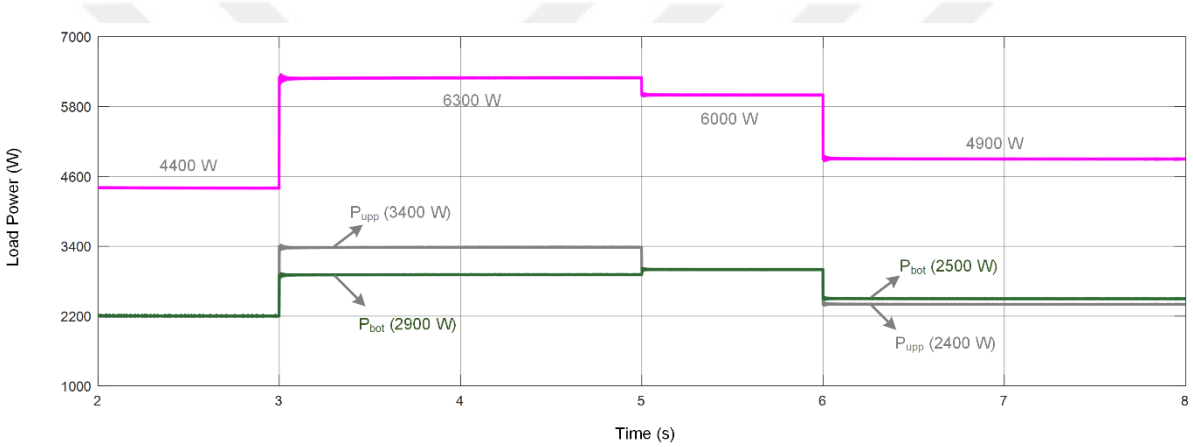

Figure 4.18. Demanded power of upper, lower and total load for Case Study 2

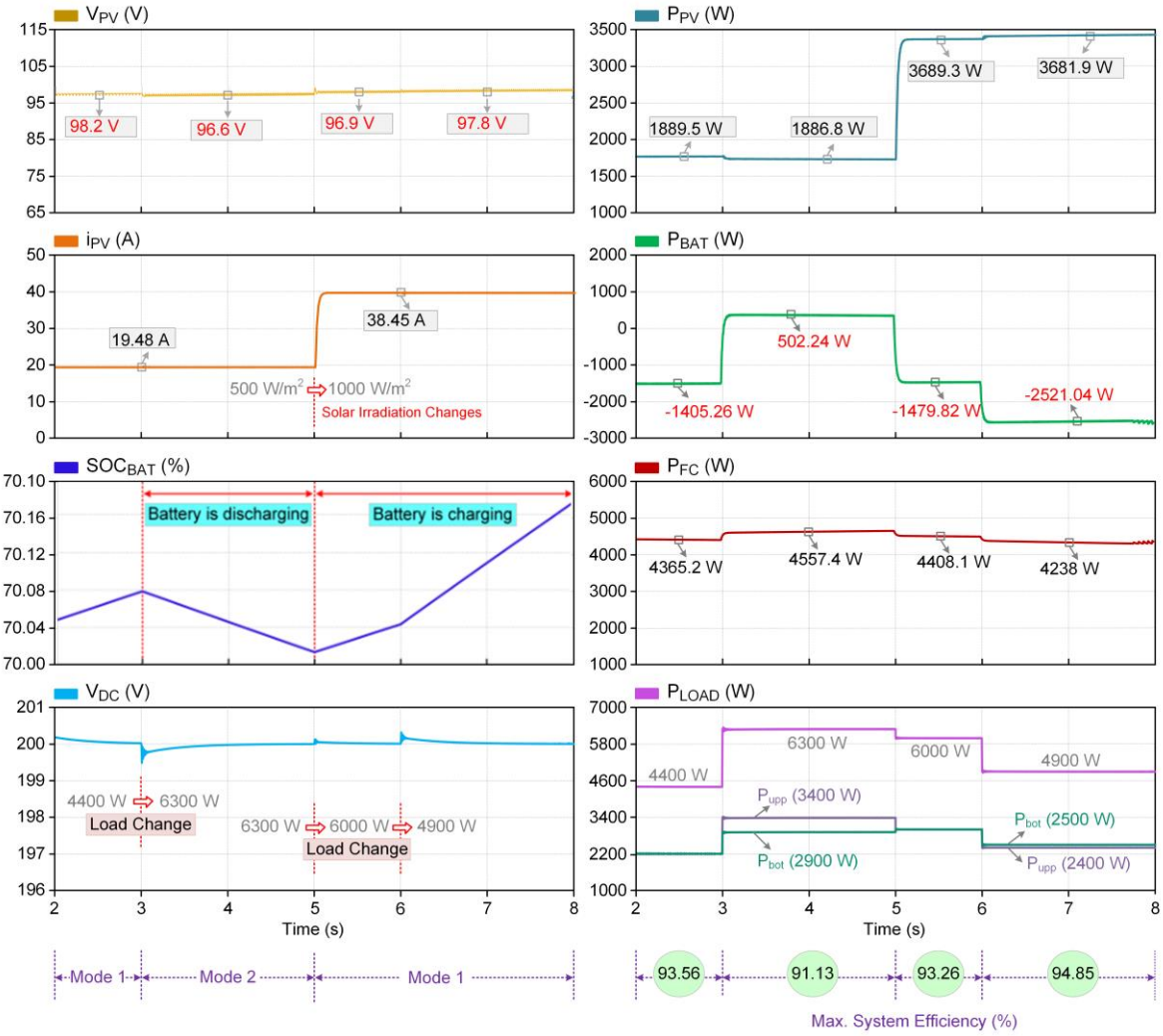

Figure 4.19. Summary of simulation results for Case Study 2

4.4. Case Study 3

The third case corresponds to mode 1 and mode 3. The performance of mode 1, mode 3, and transition performance between the related modes are investigated in this case. From t=2 s to t=5 s, the system was operated in mode 1. Furthermore, the effect of the presence and absence of PV solar irradiation on the proposed system is explored. The FC pressure value was kept constant at 0.7 bar along with this case study. The parameters of the Case Study 3 are listed in Table 4.8. In this case study, there are a total of three time intervals according to the load power variations and the presence of solar irradiation. There was an imbalance between the P_{upp} and P_{bot} powers in each interval, while the total load power was changed.

The FC voltage and current are demonstrated in Figure 4.20 and Figure 4.21 respectively. Figure 4.22 shows the SOC of the battery. The DC link voltage of the BPDCMG side is depicted in Figure 4.23. The PV power, the FC power and the battery power are shown in Figure 4.24, Figure 4.25, and Figure 4.26 respectively. In the time interval of 2-4 s, the total power demanded by the load is 4950 W. 350 W imbalance occurred between the upper and lower loads. Demanded power of load for Case Study 1 is given in Figure 4.27. The solar irradiation was kept constant at 1000 W/m^2 from t=2 to t=5. FC and PV produce the power demanded by the load, while the battery is charged. The battery is charging from t=2 s to t=5 s. As it is clearly seen from Figure 4.28., the system operates in mode 1 and the peak efficiency of the system is 93.98 % in this time interval.

As seen in Figure 4.28, the power demanded by the load increases to 5900 W at t=4 s. At t=4 s, FC current increases to 37.74 A from 36.99 A (see in Figure 4.21), and FC voltage decreases to 106.04 V from 106.51 V because of the load variation (see in Figure 4.20). The time interval of 4-5 s represents mode 1 with 1000 W/m^2 solar irradiation, 25 ^{o}C and 5900 W demand. In the time interval of 4-5 s, a 100 W imbalance occurred between the power of the upper and lower loads. From t=5 s, the battery initiates to discharge and the system operating mode switches from mode 1 to mode 3. At t=5 s, solar irradiation reduces from 1000 W/m^2 to 0 W/m^2. Therefore, PV power decreases to 0. Later, the battery power increases to -1141.73 W from -2099.65 W (see in Figure 4.25) and FC power increases to 4408.91 W from 3963.08 W (see in Figure 4.26). After t=5 s, the primary side energy units including the battery and FC supply the demanded load power. From t=5 s to t=8 s, the battery is operated in discharging mode (see in Figure 4.22).

The time interval of 5-8 s represents mode 3 with 0 W/m^2 solar irradiation, 25 ºC and 6250 W demand. 250 W imbalance occurred between the power of the upper and lower loads. From t=5 s to t=8 s, the system is operated in mode 3. It is seen that the power supplied by PV decreases to 0 depending on solar irradiation change in the time interval of 5-8 s. PV power for Case Study 3 is given in Figure 4.24.

The efficiency of the system, mode transitions, and overall variations for each time interval are detailed in Figure 4.28. As can be seen from Figure 4.28, from the beginning to the end of this case study, the effectiveness of the voltage balancer circuit was investigated and verified by giving imbalances of 350 W at the t=2 s, 100 W at the t=4 s, and 250 W at the t=5 s, respectively. In this case study, it was observed that DC microgrid voltage values are preserved when PV is disabled. Similarly, it was concluded that DC link voltage value are conserved when the imbalances are occurred between the upper and lower loads. DC link voltage for Case Study 3 is shown in Figure 4.23. FC current-voltage, the SOC of the battery, DC microgrid voltage values, and all port's power values were represented in Figure 4.20 - 4.27 for Case Study 3.

Table 4.8. Summary of Case Study 3

Time Interval	**Fuel Cell Parameters**	**PV System Parameters**	**Unbalanced Load Condition**	**Load Power (P_{upp}, P_{bot})**	**Operation Mode**
t = 2-4 s	T = 873 K P = 0.7 bar	T = 25 ºC Irr = 1000 W/m^2	Yes	P_{upp} = 2300 W P_{bot} = 2650 W	Mode 1
t = 4-5 s	T = 873 K P = 0.7 bar	T = 25 ºC Irr = 1000 W/m^2	Yes	P_{upp} = 3000 W P_{bot} = 2900 W	Mode 1
t = 5-8 s	T = 873 K P = 0.7 bar	T = 25 ºC Irr = 0 W/m^2	Yes	P_{upp} = 3250 W P_{bot} = 3000 W	Mode 3

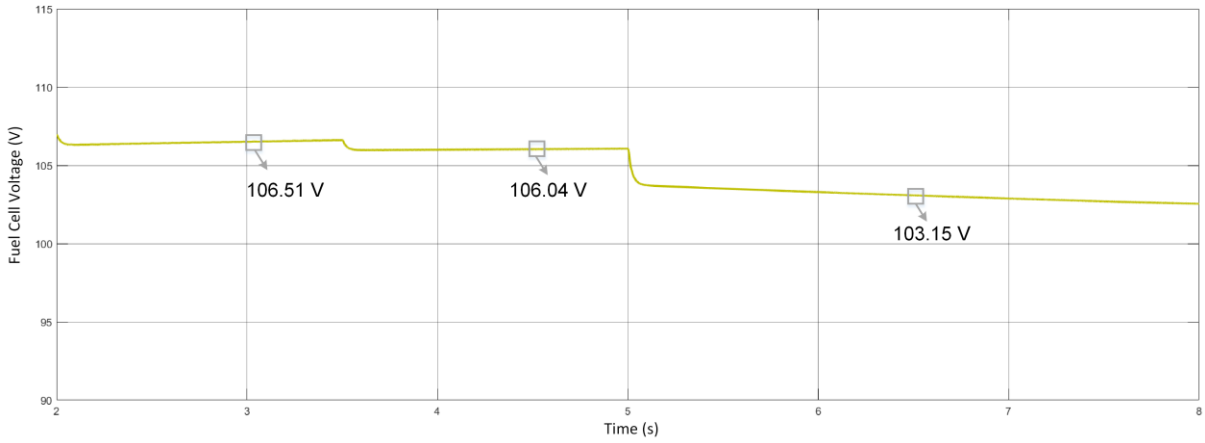

Figure 4.20. The FC voltage for Case Study 3

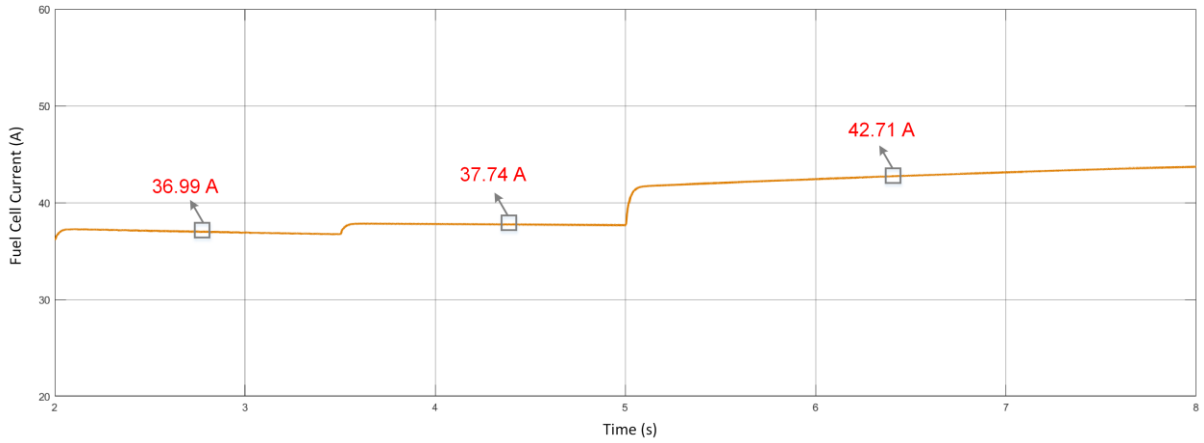

Figure 4.21. The FC current for Case Study 3

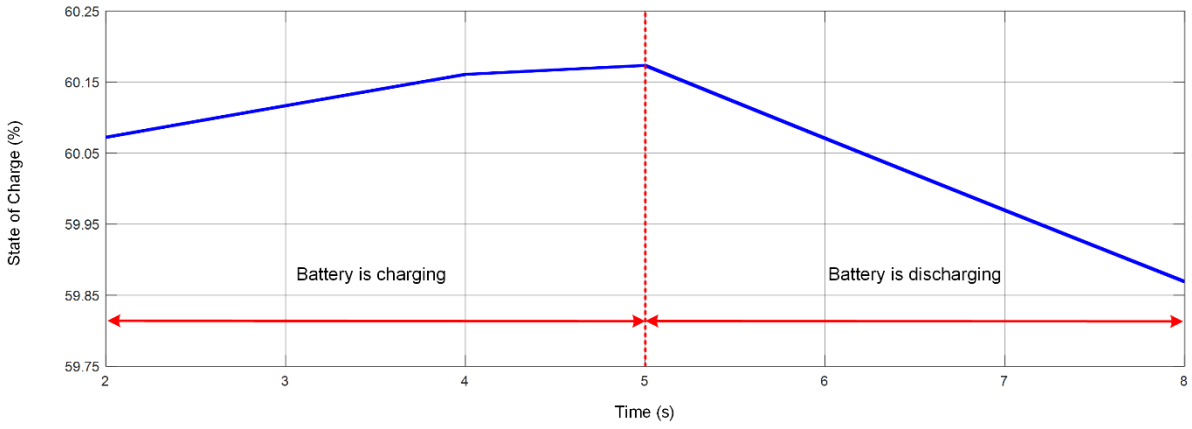

Figure 4.22. The SOC of the battery for Case Study 3

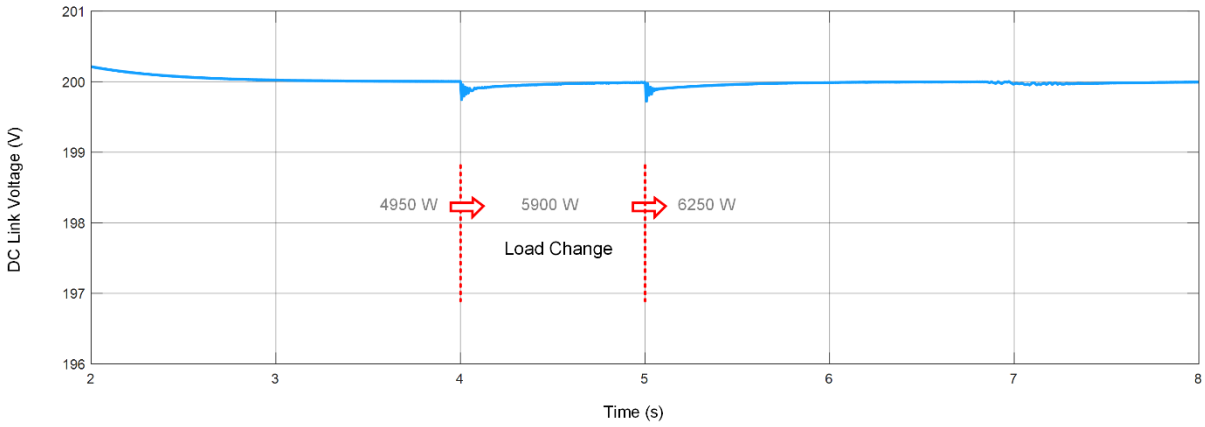

Figure 4.23. DC link voltage for Case Study 3

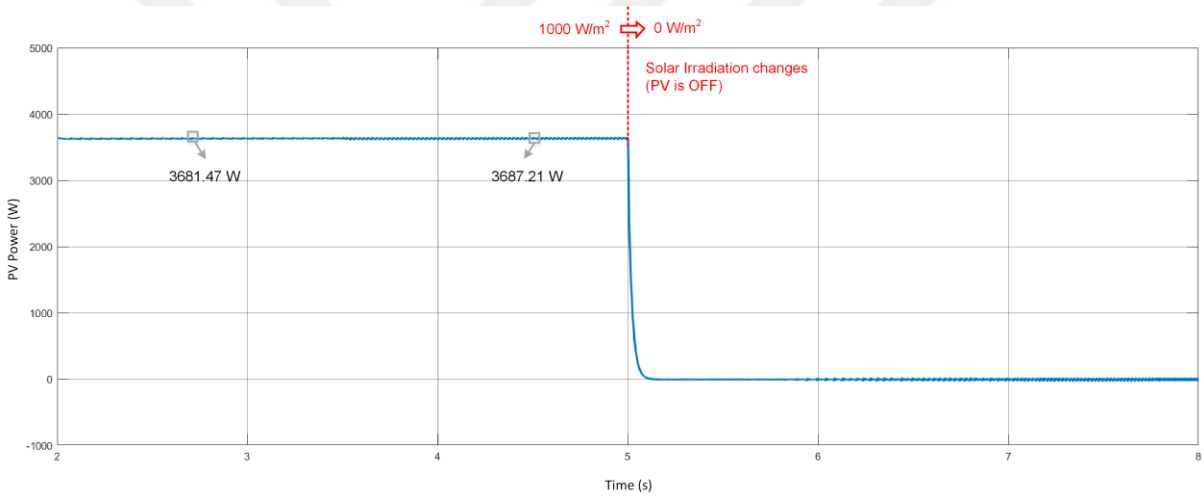

Figure 4.24. PV power for Case Study 3

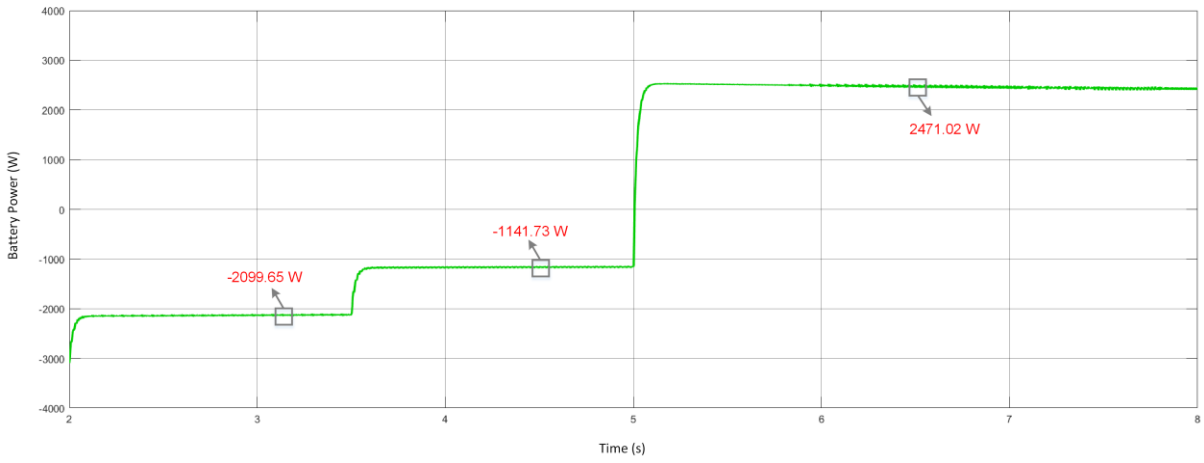

Figure 4.25. Battery power for Case Study 3

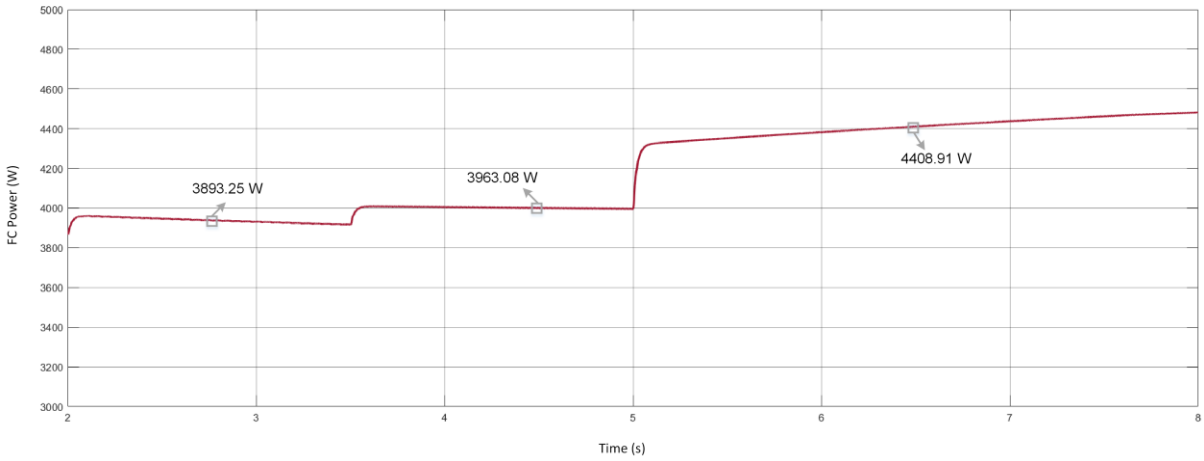

Figure 4.26. FC power for Case Study 3

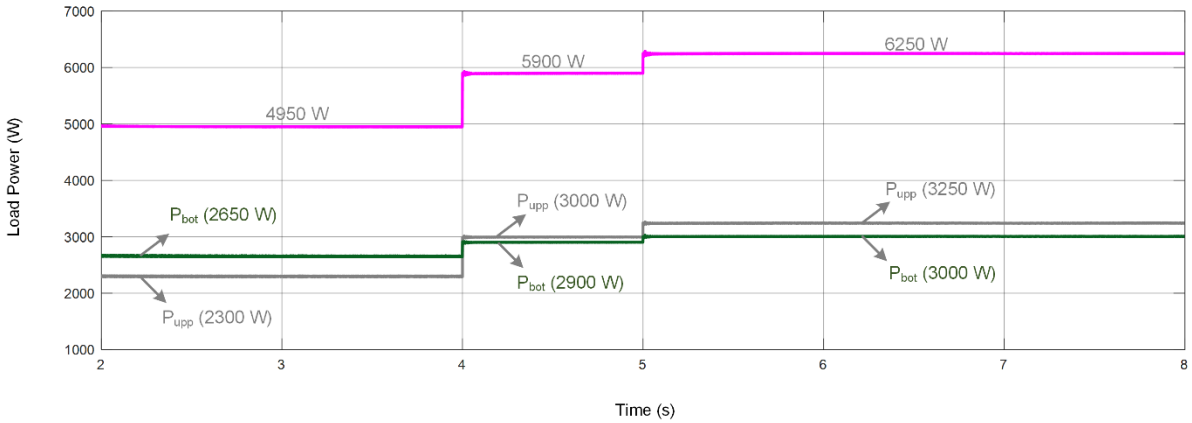

Figure 4.27. Demanded power of upper, lower and total load for Case Study 3

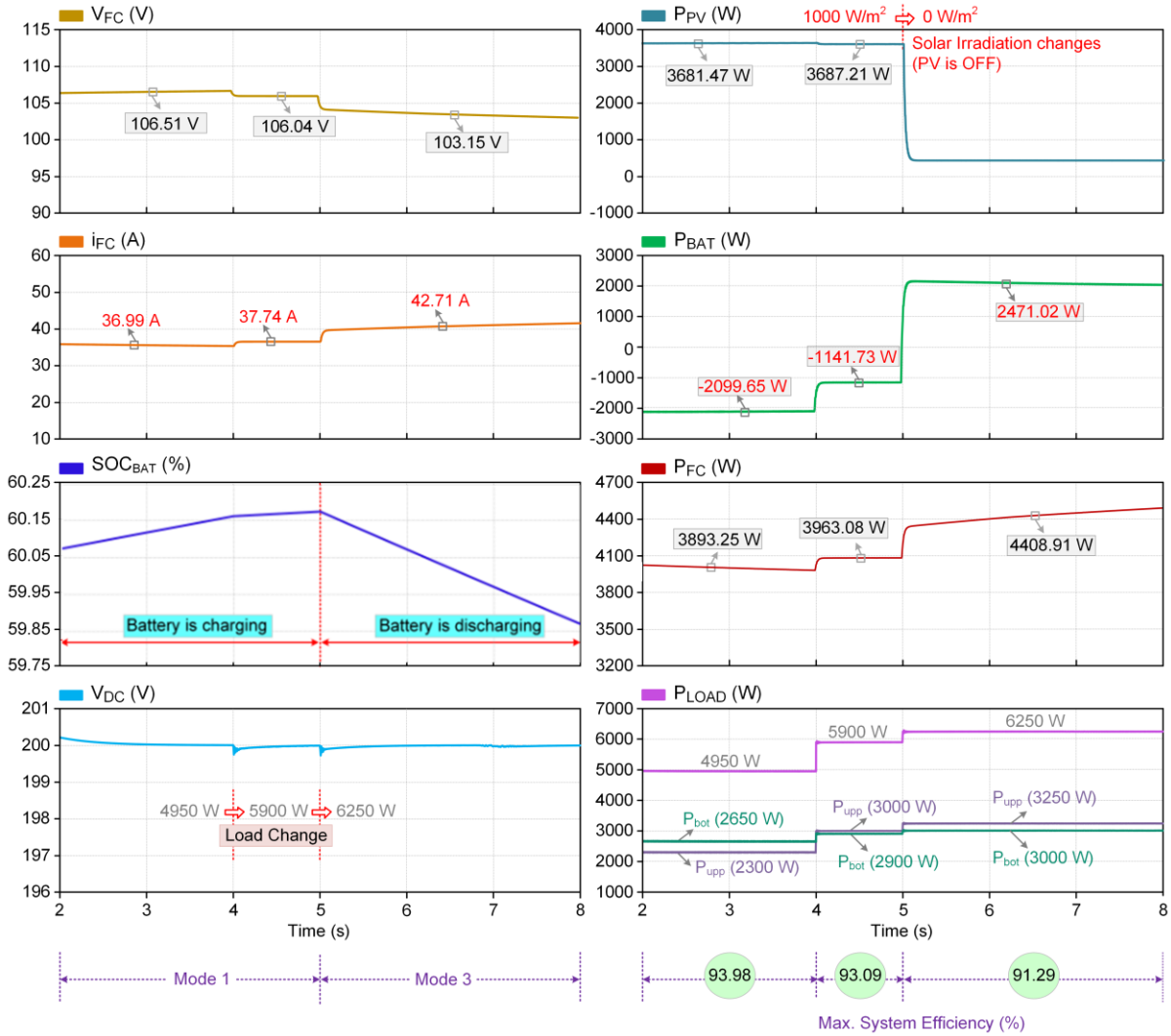

Figure 4.28. Summary of simulation results for Case Study 3

4.4. Summary

In order to evaluate the effectiveness and applicability of the proposed converter, three case studies were performed. Case studies include the variations in FC pressure and PV solar irradiation, load changes and imbalances between upper and lower loads. Case studies are formed to verify all operation modes of the proposed system.

The proposed topology can provide the following functions successfully: power flow management, renewable energy integration, compensation of bipolar output voltage differences. Figure 4.29 shows the ability of compensation of voltage differences between the upper and lower loads at the BPDCMG side for Case 2 and Case 3. Thanks to the voltage balancer circuit, V_{bot} and V_{upp} are kept constant at almost 100.235 V and 99.747 V respectively at t=4 s in the second case. On the other hand, the absence of the voltage balancer circuit or the balancing switch Q_5 is OFF, V_{bot} and V_{upp} are observed as 107.913 V and 92.049 V respectively. Hence, the difference of 15.864 V was decreased to 0.488 V by the voltage balancer circuit. Similarly, in the third case, in the case of the presence of the voltage balancer circuit, V_{bot} at t=3 s is 100.037 V, while V_{upp} is 99.979 V. On the other hand, in the case of the absence of the voltage balancer circuit, V_{bot} is 92.943 V while V_{upp} is 107.078 V. Thus, the difference of 14.135 V was decreased to 0.058 V by the voltage balancer circuit. Consequently, the ability to compensate for voltage differences on the upper and lower load sides of the BPDCMG with and without balancing is highlighted in this figure.

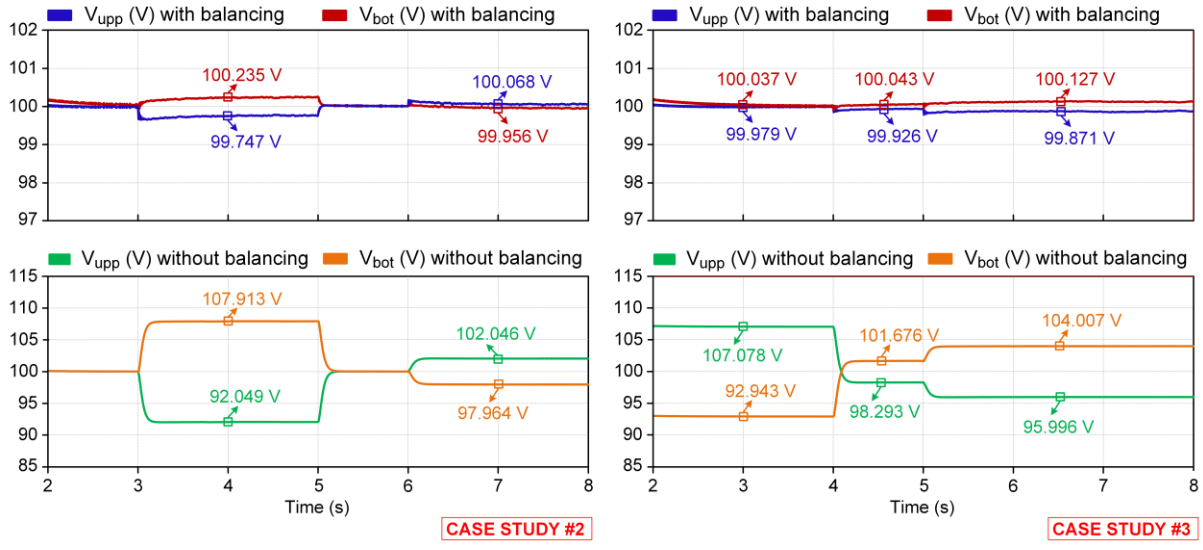

Figure 4.29. Comparison of the system performance with and without voltage balancer circuit

CONCLUSIONS

In this study, a new and versatile FPIBC configuration that combines two full-bridge converters, a resonant tank, and a voltage balancer circuit has been proposed for bipolar DC microgrid applications. The proposed converter stands out with the following advantages in comparison to other multiport converters developed for the same purpose in literature: (i) capability of integrating multi-input RESs and ESUs to bipolar DC microgrid, (ii) performing all possible power flow scenarios between the input/output ports, (iii) compensation of bipolar output voltage imbalances, (iv) providing the isolation between ports by HFT, (v) reduced number of switches, (vi) high efficiency, (vii) cost-effectiveness.

The controller detects voltage imbalances greater than 1 V and mitigates the adverse effects instantly via a voltage balancer circuit. The power flow management determines the operation mode by considering the available powers of PV, FC, and battery with the demand of the load. The performance of the proposed system and its controller under steady-state and transient conditions have been evaluated by simulation studies performed in MATLAB/Simulink software.

The effectiveness of the proposed FPIBC has been validated through comprehensive case studies involving three different modes of operation and dynamic load variations. The simulation results revealed that the system has an efficiency of at least 91.13% and the voltage imbalance is kept below 1 V during case studies. Consequently, it has been demonstrated that the proposed system operates with high efficiency, performs all the functionalities such as balancing bipolar output voltages and bidirectional power transfer between ports successfully, and responds to the transient conditions dynamically.

REFERENCES

Ahmadi, T. (2020). Voltage unbalances mitigation in bipolar DC microgrids using a novel three-port multidirectional buck–boost converter. *IET Power Electronics, May 2020,* 192–200. https://doi.org/10.1049/pel2.12024

Ahmadi, T., Rokrok, E., & Hamzeh, M. (2018a). Mitigation of voltage unbalances in bipolar DC microgrids using three-port multidirectional DC-DC converters. *Journal of Power Electronics*, *18*(4), 1223–1234. https://doi.org/10.6113/JPE.2018.18.4.1223

Ahmadi, T., Rokrok, E., & Hamzeh, M. (2018b). Supervisory control of bipolar DC microgrids equipped with three-port multidirectional DC–DC converter for efficiency and system damping optimization. *Sustainable Energy, Grids and Networks*, *16*, 327–340. https://doi.org/10.1016/j.segan.2018.10.001

Alonso, J. Marcos, Marina S. Perdigão, David Gacio Vaquero, Antonio J. Calleja, and Eduardo Sousa Saraiva. 2012. "Analysis, Design, and Experimentation on Constant-Frequency DC-DC Resonant Converters with Magnetic Control." *IEEE Transactions on Power Electronics* 27(3):1369–82. doi: 10.1109/TPEL.2011.2165083.

Askarian, I., Pahlevani, M., & Knight, A. M. (2021). Three-Port Bidirectional DC / DC Converter for DC Nanogrids. *IEEE Transactions on Power Electronics, 36*(7), 8000–8011. https://doi.org/10.1109/TPEL.2020.3046453

Chaudhury, T., & Kastha, D. (2020). A High Gain Multiport DC-DC Converter for Integrating Energy Storage Devices to DC Microgrid. *IEEE Transactions on Power Electronics*, *35*(10), 10501–10514. https://doi.org/10.1109/TPEL.2020.2977909

Cubas, J., Pindado, S., & De Manuel, C. (2014). Explicit expressions for solar panel equivalent circuit parameters based on analytical formulation and the lambert W-function. *Energies, 7*(7), 4098–4115. https://doi.org/10.3390/en7074098

Ding, Z., Yang, C., Zhang, Z., Wang, C., & Xie, S. (2014). A novel soft-switching multiport

bidirectional dc-dc converter for hybrid energy storage system. *IEEE Transactions on Power Electronics*, *29*(4), 1595–1609. https://doi.org/10.1109/TPEL.2013.2264596

Dragičević, T., Lu, X., Vasquez, J. C., & Guerrero, J. M. (2016). DC Microgrids - Part II: A Review of Power Architectures, Applications, and Standardization Issues. *IEEE Transactions on Power Electronics*, *31*(5), 3528–3549. https://doi.org/10.1109/TPEL.2015.2464277

Etxeberria, A., Vechiu, I., Camblong, H., & Vinassa, J. M. (2010). Hybrid energy storage systems for renewable energy sources integration in microgrids: A review. *2010 9th International Power and Energy Conference, IPEC 2010*, 532–537. https://doi.org/10.1109/IPECON.2010.5697053

Ferrera, M. B., Litran, S. P., Duran Aranda, E., & Andujar Marquez, J. M. (2015). A Converter for Bipolar DC Link Based on SEPIC-Cuk Combination. *IEEE Transactions on Power Electronics*, *30*(12), 6483–6487. https://doi.org/10.1109/TPEL.2015.2429745

Forrai, A., Funato, H., Yanagita, Y., & Kato, Y. (2005). Fuel-cell parameter estimation and diagnostics. *IEEE Transactions on Energy Conversion*, *20*(3), 668–675. https://doi.org/10.1109/TEC.2005.845516

Gao, F., & Rogers, D. (2018). Duty-cycle plus phase-shift control for a dual active half bridge based bipolar DC microgrid. *Conference Proceedings - IEEE Applied Power Electronics Conference and Exposition - APEC*, *2018-March*, 1479–1485. https://doi.org/10.1109/APEC.2018.8341212

Gücin, Taha Nurettin, Muhammet Biberoğlu, and Bekir Fincan. 2019. “Constant Frequency Operation of Parallel Resonant Converter for Constant-Current Constant-Voltage Battery Charger Applications.” *Journal of Modern Power Systems and Clean Energy* 7(1):186–99. doi: 10.1007/s40565-018-0403-7.

Hou, N., Song, W., & Wu, M. (2016). Minimum-Current-Stress Scheme of Dual Active Bridge DC – DC Converter With Unified Phase Shift Control. *IEEE Transactions on Power Electronics*, *31*(12), 8552–8561. https://doi.org/10.1109/TPEL.2016.2521410

İnci, M., & Türksoy, Ö. (2019). Review of fuel cells to grid interface: Configurations, technical challenges and trends. *Journal of Cleaner Production*, *213*, 1353–1370. https://doi.org/10.1016/j.jclepro.2018.12.281

Jianwu, Z., Wei, Q., Liyan, Q., & Jiao, Y. (2014). An isolated multiport DC-DC converter for simultaneous power management of multiple different renewable energy sources. *IEEE Journal of Emerging and Selected Topics in Power Electronics*, *2*(1), 70–78. https://doi.org/10.1109/JESTPE.2013.2293331

Kabalci, E., Irgan, H., & Kabalci, Y. (2018). Hybrid Microgrid System Design with Renewable Energy Sources. *Proceedings - 2018 IEEE 18th International Conference on Power Electronics and Motion Control, PEMC 2018*, 387–392. https://doi.org/10.1109/EPEPEMC.2018.8521840

Kakigano, H., Miura, Y., Ise, T., & Uchida, R. (2007). DC voltage control of the dc micro-grid for super high quality distribution. *Fourth Power Conversion Conference-NAGOYA, PCC-NAGOYA 2007 - Conference Proceedings*, 518–525. https://doi.org/10.1109/PCCON.2007.373016

Kakigano, Hiroaki, Miura, Y., & Ise, T. (2010). Low-voltage bipolar-type dc microgrid for super high quality distribution. *IEEE Transactions on Power Electronics*, *25*(12), 3066–3075. https://doi.org/10.1109/TPEL.2010.2077682

Kirubakaran, A., Jain, S., & Nema, R. K. (2009). A review on fuel cell technologies and power electronic interface. *Renewable and Sustainable Energy Reviews*, *13*(9), 2430-2440. https://doi.org/j.rser.2009.04.004

Kolahian, P., Tarzamni, H., Nikafrooz, A., & Hamzeh, M. (2019). Multi-port DC–DC converter for bipolar medium voltage DC micro-grid applications. *IET Power Electronics*, *12*(7), 1841–1849. https://doi.org/10.1049/iet-pel.2018.6031.

Li, Y. W., & Kao, C. N. (2009). An accurate power control strategy for power-electronics-interfaced distributed generation units operating in a low-voltage multibus microgrid. *IEEE Transactions on Power Electronics*, *24*(12), 2977–2988.

https://doi.org/10.1109/TPEL.2009.2022828

Li, X., & Bhat, A. K. (2010). Analysis and design of high-frequency isolated dual-bridge series resonant DC/DC converter. *IEEE Transactions on Power Electronics*, *25*(4), 850-862. https://doi.org/10.1109/TPEL.2009.2034662

Liu, C., Zhu, D., Zhang, J., Liu, H., & Cai, G. (2015). A bidirectional dual buck-boost voltage balancer with direct coupling based on a burst-mode control scheme for low-voltage bipolar-type DC microgrids. *Journal of Power Electronics*, *15*(6), 1609–1618. https://doi.org/10.6113/JPE.2015.15.6.1609

Lochala, J. A., Zhang, H., Wang, Y., Okolo, O., Li, X., & Xiao, J. (2017). Practical Challenges in Employing Graphene for Lithium-Ion Batteries and Beyond. *Small Methods*, *1*(6). https://doi.org/10.1002/smtd.201700099

Luta, D. N., & Raji, A. K. (2019) Comparing fuzzy rule-based and fractional open circuit voltage MPPT techniques in a fuel cell stack. *International Journal of Engineering&Technology, 8(4),* 402-411.

Minh, N. Q. (2004). Solid oxide fuel cell technology - Features and applications. *Solid State Ionics*, *174*(1–4), 271–277. https://doi.org/10.1016/j.ssi.2004.07.042

Mira, M. C., Zhang, Z., Knott, A., & Andersen, M. A. E. (2017). Analysis, Design, Modeling, and Control of an Interleaved-Boost Full-Bridge Three-Port Converter for Hybrid Renewable Energy Systems. *IEEE Transactions on Power Electronics*, *32*(2), 1138–1155. https://doi.org/10.1109/TPEL.2016.2549015

Mishima, T., Mizutani, H., & Nakaoka, M. (2016). A sensitivity-improved PFM LLC resonant full-bridge DC–DC converter with LC antiresonant circuitry. *IEEE Transactions on power electronics*, *32*(1), 310-324. https://doi.org/10.1109/TPEL.2016.2524640

Mohammed, S. S., & Devaraj, D. (2014). Simulation and analysis of stand-alone photovoltaic system with boost converter using MATLAB/Simulink. *2014 International Conference on*

Circuits, Power and Computing Technologies, ICCPCT 2014, *March*, 814–821. https://doi.org/10.1109/ICCPCT.2014.7054991

Mohseni, P., Hosseini, S. H., Sabahi, M., Jalilzadeh, T., & Maalandish, M. (2019). A New High Step-Up Multi-Input Multi-Output DC-DC Converter. *IEEE Transactions on Industrial Electronics*, *66*(7), 5197–5208. https://doi.org/10.1109/TIE.2018.2868281

Nasiri, A., & Jean-Pierre, G. (2020). A Multiport Bidirectional LLC Resonant Converter for Grid-Tied Photovoltaic-Battery Hybrid System. *International Journal of Renewable Energy Research*, *10*(2). https://doi.org/10.20508/ijrer.v10i2.10308.g7953

Pires, V. F., Cordeiro, A., Foito, D., & Silva, J. F. A. (2021). Dual Output and High Voltage Gain DC-DC Converter for PV and Fuel Cell Generators Connected to DC Bipolar Microgrids. *IEEE Access*, *9*, 157124–157133. https://doi.org/10.1109/ACCESS.2021.3122877

Prabhakaran, P., & Agarwal, V. (2020). Novel Boost-SEPIC Type Interleaved DC-DC Converter for Mitigation of Voltage Imbalance in a Low-Voltage Bipolar DC Microgrid. *IEEE Transactions on Industrial Electronics*, *67*(8), 6494–6504. https://doi.org/10.1109/TIE.2019.2939991

Prabhakaran, P., & Agarwal, V. (2020). Novel Four-Port DC – DC Converter for Interfacing Solar PV – Fuel Cell Hybrid Sources With Low-Voltage Bipolar DC Microgrids. *IEEE Journal of Emerging and Selected Topics in Power Electronics*, *8*(2), 1330–1340. https://doi.org/10.1109/JESTPE.2018.2885613

Rivera, S., Member, S., Wu, B., Kouro, S., Yaramasu, V., & Wang, J. (2015). Neutral Point Clamped Converter With Bipolar DC Bus. *IEEE Transactions on Industrial Electronics*, *62*(4), 1999–2009. https://doi.org/10.1109/TIE.2014.2348937

Savrun, M. M., & Atay, A. (2020). Multiport bidirectional DC-DC converter for PV powered electric vehicle equipped with battery and supercapacitor. *IET Power Electronics*, *13*(17), 3931–3939. https://doi.org/10.1049/iet-pel.2020.0759

Savrun, M. M., Köroğlu, T., Tan, A., Cuma, M. U., Bayindir, K. Ç., & Tümay, M. (2020). Isolated H-bridge DC-DC converter integrated transformerless DVR for power quality improvement. *IET Power Electronics*, *13*(5), 920–926. https://doi.org/10.1049/iet-pel.2019.0687

Stambouli, A. B., & Traversa, E. (2002). Solid oxide fuel cells (SOFCs): A review of an environmentally clean and efficient source of energy. *Renewable and Sustainable Energy Reviews*, *6*(5), 433–455. https://doi.org/10.1016/S1364-0321(02)00014-X

Swaminathan, N., & Cao, Y. (2020). An Overview of High-Conversion High-Voltage DC-DC Converters for Electrified Aviation Power Distribution System. *IEEE Transactions on Transportation Electrification*, *6*(4), 1740–1754. https://doi.org/10.1109/TTE.2020.3009152

Tan, N. M. L., Abe, T., & Akagi, H. (2012). Design and performance of a bidirectional isolated DC-DC converter for a battery energy storage system. *IEEE Transactions on Power Electronics*, *27*(3), 1237–1248. https://doi.org/10.1109/TPEL.2011.2108317

Tavakoli, S. D., Khajesalehi, J., Hamzeh, M., & Sheshyekani, K. (2016). Decentralised voltage balancing in bipolar dc microgrids equipped with trans-z-source interlinking converter. *IET Renewable Power Generation*, *10*(5), 703–712. https://doi.org/10.1049/iet-rpg.2015.0222

Tian, Q., Zhou, G., Leng, M., Xu, G., & Fan, X. (2020). A Nonisolated Symmetric Bipolar Output Four-Port Converter Interfacing PV-Battery System. *IEEE Transactions on Power Electronics*, *35*(11), 11731–11744. https://doi.org/10.1109/TPEL.2020.2983113

Tian, Q., Zhou, G., Li, H., Yang, Y., & Zhou, D. (2022). Symmetrical Bipolar Output Isolated Four-Port Converters Based on Center-Tapped Winding for Bipolar DC Bus Applications. *IEEE Transactions on Power Electronics*, *37*(2), 2338–2351. https://doi.org/10.1109/TPEL.2021.3107154

Vettuparambil, A., Chatterjee, K., & Fernandes, B. G. (2021). A Multiport Converter Interfacing Solar Photovoltaic Modules and Energy Storage with DC Microgrid. *IEEE Transactions on Industrial Electronics*, *68*(4), 3113–3123.

https://doi.org/10.1109/TIE.2020.2978709

Vettuparambil, A., Chatterjee, K., & Fernandes, B. G. (2022). Dual-Active-Bridge-Based Multiport Converter with Split DC Links. *IEEE Transactions on Industrial Electronics*, *69*(1), 485–494. https://doi.org/10.1109/TIE.2021.3051576

Wang, F., Lei, Z., Xu, X., & Shu, X. (2017). Topology deduction and analysis of voltage balancers for DC microgrid. *IEEE Journal of Emerging and Selected Topics in Power Electronics*, *5*(2), 672–680. https://doi.org/10.1109/JESTPE.2016.2638959

Wu, H., Jia, Y., Yang, F., Zhu, L., & Xing, Y. (2020). Two-Stage Isolated Bidirectional DC-AC Converters with Three-Port Converters and Two DC Buses. *IEEE Journal of Emerging and Selected Topics in Power Electronics*, *8*(4), 4428–4439. https://doi.org/10.1109/JESTPE.2019.2936145

Wu, H., Sun, K., Zhu, L., & Xing, Y. (2016). An Interleaved Half-Bridge Three-Port Converter With Enhanced Power Transfer Capability Using Three-Leg Rectifier for Renewable Energy Applications. *IEEE Journal of Emerging and Selected Topics in Power Electronics*, *4*(2), 606–616. https://doi.org/10.1109/JESTPE.2015.2478140

Zeng, J., Du, X., & Yang, Z. (2021). A Multiport Bidirectional DC-DC Converter for Hybrid Renewable Energy System Integration. *IEEE Transactions on Power Electronics*, *36*(11), 12281–12291. https://doi.org/10.1109/TPEL.2021.3082427

Zeng, J., Qiao, W., & Qu, L. (2015). An Isolated Three-Port Bidirectional DC-DC Converter for Photovoltaic Systems With Energy Storage. *IEEE Transactions on Industry Applications*, *51*(4), 3493–3503. https://doi.org/10.1109/TIA.2015.2399613

Zhang, J., Jiang, W., Jiang, T., Shao, S., Sun, Y., Hu, B., & Zhang, J. (2019). A Three-Port LLC Resonant DC/DC Converter. *IEEE Journal of Emerging and Selected Topics in Power Electronics*, *7*(4), 2513–2524. https://doi.org/10.1109/JESTPE.2019.2902425

Zhang, N., Sutanto, D., & Muttaqi, K. M. (2016). A review of topologies of three-port DC-DC

converters for the integration of renewable energy and energy storage system. *Renewable and Sustainable Energy Reviews*, *56*, 388–401. https://doi.org/10.1016/j.rser.2015.11.079

Zhu, H., Zhang, D., Athab, H. S., Wu, B., & Gu, Y. (2015). PV isolated three-port converter and energy-balancing control method for PV-battery power supply applications. *IEEE Transactions on Industrial Electronics*, *62*(6), 3595–3606. https://doi.org/10.1109/TIE.2014.2378752